COHERENCE PROPERTIES OF OPTICAL NEAR-FIELDS

by

ADELA M. APOSTOL
MS Optics, College of Optics and Photonics-CREOL, University of Central Florida, 2001
B.S. Physics, Bucharest University, Romania 1993

A dissertation submitted in partial fulfillment of the requirements
for the degree of Doctor of Philosophy
in the College of Optics and Photonics
at the University of Central Florida
Orlando, Florida

Spring Term
2005

Major Professor: Aristide Dogariu

ABSTRACT

Next generation photonics-based technologies will ultimately rely on novel materials and devices. For this purpose, phenomena at subwavelength scales are being studied to advance both fundamental knowledge and experimental capabilities. In this dissertation, concepts specific to near-field optics and experimental capabilities specific to near-field microscopy are used to investigate various aspects of the statistical properties of random electromagnetic fields in the vicinity of optically inhomogeneous media which emit or scatter radiation. The properties of such fields are being characterized within the frame of the coherence theory. While successful in describing the far-field properties of optical fields, the fundamental results of the conventional coherence theory disregard the contribution of short-range evanescent waves. Nonetheless, the specific features of random fields at subwavelength distances from interfaces of real media are influenced by the presence of evanescent waves because, in this case, both propagating and nonpropagating components contribute to the detectable properties of the radiation. In our studies, we have fully accounted for both contributions and, as a result, different surface and subsurface characteristics of inhomogeneous media could be explored.

We investigated different properties of random optical near-fields which exhibit either Gaussian or non-Gaussian statistics. We have demonstrated that characteristics of optical radiation such as first- and second-order statistics of intensity and the spectral density in the vicinity of random media are all determined by both evanescent waves contribution and the statistical properties of the physical interface. For instance, we quantified the subtle differences which exist between the near- and far-field spectra of radiation and we brought the first experimental evidence that, contrary to the predictions of the conventional coherence theory, the values of coherence length in the near field depend on the distance from the interface and, moreover, they can be smaller than the wavelength of light.

The results included in this dissertation demonstrate that the statistical properties of the electromagnetic fields which exist in the close proximity of inhomogeneous media can be used to extract structural information. They also suggest the possibility to adjust the coherence properties of the emitted radiation by modifying the statistical properties of the interfaces. Understanding the random interference phenomena in the near-field could also lead to new possibilities for surface and subsurface diagnostics of inhomogeneous media. In addition, controlling the statistical properties of radiation at subwavelength scales should be of paramount importance in the design of miniaturized optical sources, detectors and sensors.

In the memory of my mother, Elisabeta Apostol

ACKNOWLEDGEMENTS

I would never have been able to complete this work without the help of some wonderful people. It is my greatest pleasure to recognize those who have supported me and shared with me the stress, the worries and the joy of this journey.

Nothing would have been possible without the dedication, patience and great intuition of my adviser, Dr. Aristide Dogariu. I thank him for believing in me and for guiding and supporting me throughout the years. I would also like to express my deepest gratitude to him for the opportunity and the freedom to explore the world of "near-field optics".

I am thankful to the amazing minds of the "Random" team. Being a part of this group has been both a great honor and a source of joy.

Special thanks to my best friends: to Adrian for always being there caring for me, to Claudia for her wise advice, to Marc for loving me the way I am, to Nicoleta for being warm and trustful and to Waleed for his support and encouragement along the way.

My deepest thanks go to my family. "Multumesc" to my sister Diana for her unconditional love and support and to my nephew Mihnea for bringing so much joy into my life. To my parents, "multumesc" for giving me "wings" and strength "to fly".

If I made it to the end of this voyage, it is mostly because my mother's love, spirit and memory have always been with me. Thank you mom, I love you, I miss you and I dedicate this to you.

TABLE OF CONTENTS

LIST OF FIGURES

CHAPTER ONE: INTRODUCTION

Coherence theory offers the framework for discussing the statistical properties of random fields [1]. Thermal fields are typical examples of random fields as they are produced by a large number of uncorrelated radiative desexcitations. On the other hand, a fully coherent field can acquire a random nature after being scattered by an inhomogeneous system. The state of coherence of an optical field is measured by the degree of crosscorrelation of the field at different points in space and/or different times; one can therefore distinguish between spatial and temporal coherence properties. In what follows, we will be mostly concerned with the spatial coherence of the light emerging or scattered from a highly inhomogeneous medium. A typical manifestation of the properties of such optical fields is their far-field intensity variation, the so-called speckle patterns, which have been studied in detail [2] in the past. Little is known, however, about the random field distribution close to the surface of an optically inhomogeneous medium where the presence of contributions from the evanescent waves can modify the statistical properties of the field. The importance of evanescent waves was ignored for a long time in optical and surface physics until the development of scanning near-field optical microscopes. The goal of this thesis is to elucidate the characteristics of the fluctuating optical fields in

the vicinity of a highly inhomogeneous medium taking into consideration not only the propagating waves contribution but also the evanescent ones. As will be suggested in the followings, the study of speckle phenomena in the near field could lead to new possibilities for surface and subsurface diagnostics of inhomogeneous media. Such intrinsically passive characterization tools should also be of practical use in biological applications.

Understanding the statistical properties of radiation and the radiative transfer over length scales smaller than the wavelength will impact the design of efficient coupling into and out of novel nanostructured materials for compact photonic systems. In addition, manipulating the coherence properties could lead to the development of new concepts for robust, integrated sensing techniques with resolution below the propagating light's wavelength. The next generation of optical sources and sensors will necessarily be developed at these dimensions in order to address the ever-increasing demands for miniaturization, flexibility, and efficiency.

Chapter 1 presents an introduction to the properties of fluctuating optical fields and their interaction with optically inhomogeneous media. As a result of this interaction, a random intensity pattern forms inside and outside the medium. When one accounts just for the propagating waves, the extension of the spatial correlations of the speckle pattern is limited to the value of the wavelength. However, the study of coherence phenomena at subwavelength scales requires that the evanescent waves contributions be fully taken into consideration. Therefore, Chapter 1 also introduces the basic concepts regarding the optical near-fields, more exactly how they can be produced and detected. Different experimental techniques specific to near-field optics are then briefly discussed. In particular,

various capabilities of a near-field scanning optical microscope (NSOM) are demonstrated and an example of an imaging application for the study of biological processes is illustrated.

The NSOM's superresolution capability of detecting simultaneously the topographic information and the optical signals the are exploited in the next chapters for studying in detail the statistical properties of radiation scattered by a randomly inhomogeneous media.

In Chapter 2 a short description of practical situations where scattering media are globally excited and of the random media under the study are given. The evanescent waves contribution to the total detected signal and the regime of Gaussian statistics of intensity fluctuations are experimentally demonstrated.

Chapter 3 is dedicated to the study of the characteristics of second-order correlations of optical fields in the proximity of a random medium. The work presented in this chapter proves that the spatial coherence length in the near-field of a random medium depends on the distance from the physical interface and also on the surface characteristics. It also brings the first experimental evidence that, at distances smaller that the wavelength of light, contrary to the predictions of conventional coherence theory, the coherence length can be smaller than the wavelength of light. Moreover, we shown in this chapter that, at several wavelengths away from a surface, the spatial extent of the field correlations relates with the statistical properties the physical interface. The surface of the random medium can be considered being equivalent with a homogenous, planar, infinite source of radiation. By taking into consideration the contribution of the evanescent components of

the fields to the cross-spectral density function, we develop a model that quantitatively describes the experimental results of both Chapter 3 and Chapter 4

Chapter 4 investigates another physical property of random fields in vicinity of the inhomogeneous media, namely their spectral density. Measuring the subtle differences between the near- and far-field spectrum of light we will show that the red shift of the near-field spectra is determined by the distance from the physical interface and by the coherence of the equivalent source of optical radiation. This particular characteristic of the near-field spectra of light may be also used to find information about the surface statistics.

Chapter 5 deals with the situation where the highly scattering medium is locally excited in a reflection-illumination geometry of an NSOM. We will prove that in this case, the near-field speckle pattern in the neighborhood of the random medium is governed by non-Gaussian statistics. Therefore, the optical contrast is significantly smaller than unity and is dependent on the physical properties of the interface. This practical situation allows using the first-order intensity statistics for the study of surface and subsurface properties of the random media.

Finally, the conclusions and a summary of the original contributions of this thesis will be presented in Chapter 6.

1.1. Fluctuating optical fields

1.1.1 Field correlations in the space-frequency domain

Real electromagnetic fields are fluctuating. Most optical experiments rely on interference phenomena which, in turn, depend on the correlations that exist between the light fluctuations. The purpose of this section is to introduce some of the basic concepts of field correlations in the space-frequency domain which will be lately used to describe different aspects of the near-field speckle phenomena.

Let us introduce the analytical signal $\widetilde{E}(\mathbf{r},t)$ representing the fluctuating optical field at the space-time point $(\mathbf{r},t)$, and its Fourier representation [1]

$$\widetilde{E}(\mathbf{r},t) = \int_0^{+\infty} E(\mathbf{r},\upsilon)\cdot\exp(-2\pi i\upsilon t)d\upsilon. \tag{1}$$

The cross-spectral density function $W(\mathbf{r}_1,\mathbf{r}_2,\upsilon)$ of the light at points $\mathbf{r}_1$ and $\mathbf{r}_2$ at frequency υ can be defined as the ensemble average over the different realizations of the fluctuating field

$$W(\mathbf{r}_1,\mathbf{r}_2,\upsilon)\delta(\upsilon-\upsilon') = \langle E^*(\mathbf{r}_1,\upsilon)\cdot E(\mathbf{r}_2,\upsilon')\rangle \tag{2}$$

where * denotes the complex conjugate and δ is the Dirac function.

A basic theorem of stochastic processes called the generalized Wiener-Khintchine theorem states that, for stationary processes, the cross-spectral density function $W(\mathbf{r}_1,\mathbf{r}_2,\upsilon)$ of the random process and the mutual coherence function, $\Gamma(\mathbf{r}_1,\mathbf{r}_2,\tau)$ form a Fourier transform pair:

$$\begin{aligned} \Gamma(\mathbf{r}_1, \mathbf{r}_2, \tau) &= \int_0^\infty W(\mathbf{r}_1, \mathbf{r}_2, \upsilon) \exp(-2\pi i \upsilon \tau) d\upsilon \\ W(\mathbf{r}_1, \mathbf{r}_2, \upsilon) &= \int_{-\infty}^\infty \Gamma(\mathbf{r}_1, \mathbf{r}_2, \tau) \exp(2\pi i \upsilon \tau) d\tau, \end{aligned} \tag{3}$$

where the mutual coherence function, defined as the ensemble averaged cross-correlation

$$\Gamma(\mathbf{r}_1, \mathbf{r}_2, \tau) = \left\langle \widetilde{E}^*(\mathbf{r}_1, t) \cdot \widetilde{E}(\mathbf{r}_2, t+\tau) \right\rangle \tag{4}$$

is the central quantity of the elementary theory of optical coherence of radiation.

In the special case when $\mathbf{r}_1$ coincides with $\mathbf{r}_2$, the cross spectral density function becomes the spectral density

$$S(\mathbf{r}, \upsilon) = W(\mathbf{r}, \mathbf{r}, \upsilon). \tag{5}$$

expressing the spectral content of radiation in the point $\mathbf{r}$.

By normalizing $W(\mathbf{r}_1, \mathbf{r}_2, \upsilon)$, one obtains the expression for the spectral degree of coherence at frequency υ [1]

$$\mu(\mathbf{r}_1, \mathbf{r}_2, \upsilon) = \frac{W(\mathbf{r}_1, \mathbf{r}_2, \upsilon)}{\sqrt{W(\mathbf{r}_1, \mathbf{r}_1, \upsilon)}\sqrt{W(\mathbf{r}_2, \mathbf{r}_2, \upsilon)}} = \frac{W(\mathbf{r}_1, \mathbf{r}_2, \upsilon)}{\sqrt{S(\mathbf{r}_1, \upsilon)}\sqrt{S(\mathbf{r}_2, \upsilon)}} \tag{6}$$

It can be shown that $0 \leq |\mu(\mathbf{r}_1, \mathbf{r}_2, \upsilon)| \leq 1$ for any $\mathbf{r}_1, \mathbf{r}_2$ and υ [1].

1.1.2 Field correlations inside and outside a random medium

When optical radiation propagates through a randomly inhomogeneous medium, the multiple scattering events randomize the directions and the phases of the waves. The radiation originating from such a system is commonly regarded as spatially incoherent. It was a long-time belief that multiple scattering washes out all the structural information and that such a highly inhomogeneous medium would behave as a perfect lambertian diffuser. The scattered waves interfere with each other and, as a result, a certain random intensity pattern is formed. The properties of this random pattern can be described using the definitions presented above.

The interaction between optical waves and random media has been systematically investigated and it is now well understood that the familiar appearance of speckle patterns is due to the short-range correlations of the waves transmitted or reflected from the random medium. The field correlations in the bulk of a random medium at a given frequency as $C(\mathbf{R}) = \langle E(\mathbf{r})^* E(\mathbf{r}+\mathbf{R})\rangle$, have been under scrutiny for quite some time [3]. Using diagrammatic calculations and assuming a constant photon density, Shapiro [3] found that the optical field at points separated by a distance R in a highly random volume correlates like

$$C(R) = [\sin(kR)/(kR)] \exp(-R/2l), \tag{7}$$

where l is the scattering mean free path and $k = 2\pi/\lambda$. In the weak scattering regime, $kl > 1$, the speckle size in the bulk of a multiple scattering medium is of the order of λ. Based on radiative transnsfer arguments, Freund [4] finds that the field correlation at the

surface of a random medium is given by:

$$C(R) = 2\left[\Delta \sin(kR)/(kR) + J_1(kR)/(kR)\right]/(1+2\Delta) \tag{8}$$

with Δ being a factor of the order of unity. Again, the wavelength of light determines the size of the field correlations and it is worth mentioning that similar conclusion is reached when the coherence properties of two-dimensional statistically homogeneous sources are evaluated [5]. It would appear therefore that the extension of the spatial correlations is limited to the value of the wavelength. Of course, this treatment does not account for the existence of significant evanescent contributions to the field distribution at the surface and, therefore, fails to explain the coherence effects in the near field of a random medium. First- and second-order statistics of far-field speckle pattern have been extensively investigated [2]. However, coherence effects at subwavelength scales required evanescent waves contributions to be accounted for.

An alternative description can be developed which considers the surface of the random medium as being equivalent to an homogeneous, planar, statistically stationary source of optical radiation [5]. However, it is important to realize that real scattering media are bounded by interfaces which are rough on the scale of the wavelength and this may affect the field correlation in the neighborhood of the surface. The effect of a real surface can be accounted for by considering an "effective" planar interface that radiates an intensity with an angular distribution different from the classical cosine dependence predicted by the diffusion theory [6]. These approaches will be extensively used in the following chapters to describe the characteristics of the fluctuating optical fields in the neighborhood of random media.

In order to explore the coherence properties in the proximity of an interface, one must measure the field's local properties by scanning a probe across the surface. So far, near-field scanning techniques have been used only to investigate different aspects of electromagnetic fields in close proximity of interfaces aiming primarily at extending the spatial resolution of various optical microscopies. In this thesis, near-field experimental techniques will be employed to study specific effects of field correlations in the vicinity of interfaces. We are going to show how different experimental approaches specific to near-field optics can be used to determine the relation between the field statistics close to the surface of a random medium and the statistical properties of its physical interface.

1.2 Optical near fields: existence and detection

The near-field can be considered as the outside extension of the field existing inside a given medium. Basically, the near-fields follows from the linear, homogeneous and isotropic properties of the space-time that impose a continuous variation of field amplitudes and energies across interfaces.

Optical near-fields belong to the class of surface near-fields that can only be produced by applying an external excitation. The simplest method of producing them is to illuminate a dielectric interface under conditions of total internal reflection (TIR). In this configuration, the illuminating field is incident onto the surface at an angle larger that the critical angle such that the excitation field above the surface becomes an evanescent surface wave with an amplitude which decays exponentially along the direction perpendicular to the interface. An evanescent (inhomogeneous) plane wave, as opposed to a propagating (homogeneous) wave, is a wave whose planes of constant amplitude and constant phase

do not coincide, but cross each other at a certain angle. In most cases, the amplitude of the near-field decays very rapidly along the direction perpendicular to the interface giving rise to the so-called evanescent wave character of the near-field.

The electric field in a plane $z = z_o$ above the highest point of the sample surface can be represented by its angular spectrum, i.e. the plane-wave expansion

$$E(\mathbf{r}_\parallel, t) = \int_0^{+\infty} e(\mathbf{k}_\parallel) \cdot \exp(i\mathbf{k}_\parallel \mathbf{r}_\parallel + i\gamma z_o) d\mathbf{k}_\parallel \tag{9}$$

where $\mathbf{r}_\parallel = (x, y)$, $\mathbf{k}_\parallel = (k_x, k_y)$, $k_o = \omega/c$ and $\gamma = (k_o^2 - \mathbf{k}_\parallel^2)^{1/2}$ is the z component of the wave vector $\mathbf{k}$, with the determination $\mathrm{Re}(\gamma) > 0$, $\mathrm{Im}(\gamma) > 0$. A temporal dependence $\exp(-i\omega t)$ is assumed and omitted throughout this section.

In Equation (9), the field is represented as a superposition of plane waves, each of them having a complex amplitude $e(\mathbf{k}_\parallel)$ and a wave vector $\mathbf{k} = (\mathbf{k}_\parallel, \gamma)$. In terms of Fourier analysis, $e(\mathbf{k}_\parallel) \cdot \exp(i\gamma z_o)$ represents the Fourier transform of the field in the plane $z = z_o$. For low spatial frequencies $\left|\mathbf{k}_\parallel\right| \leq k_o, \gamma$ is real and the exponential is only a phase factor. The corresponding plane waves are homogeneous, and propagate away from the surface, in the direction defined by the wave vector $\mathbf{k}$. For high spatial frequencies $\left|\mathbf{k}_\parallel\right| > k_o$, γ is purely imaginary and the exponential term acts as an attenuation factor $\exp(-\mathrm{Im}(\gamma) z_o)$. The corresponding plane waves are evanescent, propagate along the xy plane and are attenuated exponentially in the z direction. The decay length along z is given by $1/\mathrm{Im}(\gamma)$. This can happen, for example, in situations when a dielectric is illuminated in TIR as already mentioned above, or when the light is emitted through an

aperture smaller than the wavelength of light. This last case of light emission through a very small tip will be discussed in more detail in the next section.

The physics of optical evanescent waves is the central concept used in the near-field optics (NFO). Because of their evanescence, the inhomogeneous waves cannot be used for transferring optical information over any appreciable distance. Therefore, they always have to be used in combination with homogeneous waves in such a way that propagating waves are converted into evanescent waves or vice versa. Historically, in the optical domain, the first experiment of near-field detection was reported three centuries ago by Isaac Newton. He observed for the first time that the total reflection of a light beam on a dielectric interface could be frustrated by approaching a second glass prism close to the interface. In this case, the beam intensity seems to be captured by the second material and decays exponentially when increasing the spacing between the two bodies. This phenomenon is fully explained by the classical Maxwell electromagnetic theory by applying standard boundary conditions over the two interacting surfaces. Nowadays, very small probes are used for local detection of optical near-fields. NFO instrumentation provides super-resolved images, being probably the most powerful tool available for subwavelength characterization of optical fields.

Considering the angular spectrum (Equation (9)) as a two-dimensional Fourier transform in the xy plane, the widths Δx and Δy of the field in the direct space and the widths Δk_x and Δk_y obey the reciprocity relation

$$\Delta x \Delta k_x \geqslant 2\pi;\ \Delta y \Delta k_y \geqslant 2\pi. \tag{10}$$

According with this relation and assuming that one is able to detect the evanescent waves with the angular spectrum corresponding to a purely imaginary value of γ, the widths Δk_x and Δk_y may become as large as desired (and larger than $2k_o$). Thus, the lateral resolution which is described by $\Delta x = 2\pi/\Delta k_x$ and $\Delta y = 2\pi/\Delta k_y$ can become very small. Of course, in practice, this possibility of increasing arbitrarily the lateral resolution depends on the ability of collecting the light corresponding to imaginary value of γ. As we have seen before, this light is contained in the evanescent components of the angular spectrum and remains bounded to the sample surface. Thus, the widths Δk_x and Δk_y that are actually achievable will depend on the distance where the detection is performed. As we will see in the next section, in practice, the achievable resolution may be limited not only by the distance between the detector and the surface sample but also by the size of the detector.

1.3 Experimental techniques

An optical image with a resolution well below the diffraction limit can be obtained using a sub-wavelength probe which is scanned close to the sample surface. This nanometer size probe can be a light source, a detector or a scatterer [7],[8]. A sub-wavelength light source or detector can be created by using an aperture significantly smaller than the diffraction limit [9]-[14]. The concept of the evanescent waves and the resolution limit introduced in previous section are useful in understanding the ability of the near field optical techniques to produce superresolution.

Different set-ups working in the near-field have been designed for producing images with superresolution. The techniques can be roughly divided into two categories. Super-

resolution may be obtained by detecting the far-field light scattered by a small part of the sample under very localized illumination: this is the so called Illumination Mode Near-field Scanning Optical Microscope. Another approach is based on detecting the near field very close to the surface of the media which is illuminated from the far field. This is the Collection Mode Near-field Scanning Optical Microscope. Alternatively, a small scatterer may be introduced in the near-field so that the light scatter by it can be detected in the far field. This procedure is called Apertureless Near-field Scanning Optical Microscopy.

As illustrated in Figure 1a, the super-resolution capability of the illumination mode NSOM comes from the high localization of the source. The field exiting the aperture is localized in a subwavelength area. The closer the tip is, the more important is its evanescent contribution leading to a more confined illumination. The aperture approaches a sample containing subwavelength variations in the topography and/or in the optical properties. This sample scatters the illuminating field and during the scattering process, some of the evanescent waves are converted into homogeneous waves, which are then detected in the far field.

In so collection-mode scheme, the light scattered by the sample contain evanescent components. As illustrated in Figure 1b, these evanescent waves are collected by the tip of an optical fiber. In fact, the scattering process at the tip realizes the coupling between the near field and the propagating modes inside the fiber. Once again, evanescent waves are converted into propagating waves which are then detected in the far field.

In the so-called apertureless technique, depicted in Figure 1c, an additional mechanism is added to convert evanescent waves into propagating waves. This is preceded

by scattering on the tip and can work as a "two ways" conversion of homogeneous into inhomogeneous components of an optical field. A small probe, which can be a metallic or dielectric sharp tip, scatters the incident light and creates evanescent waves which illuminate the sample. The scattering process in the sample converts then a part of these illuminating evanescent waves into propagating ones, which also contributes to the signal detected in the far-field.

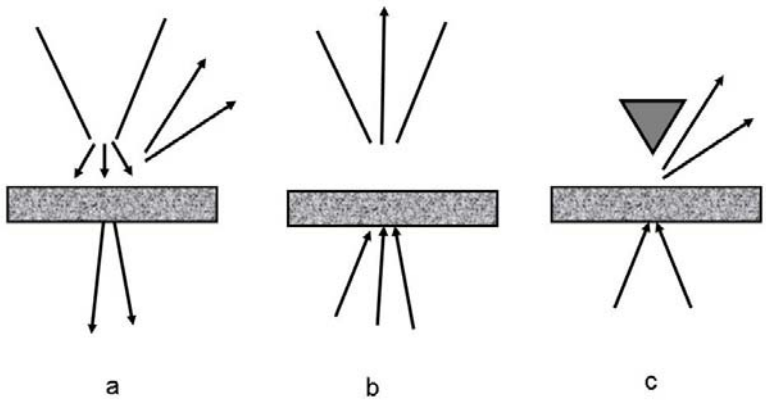

Figure 1: a) NSOM in illumination mode of operation; b) NSOM in collection mode of operation; c) apertureless NSOM

Depending on the specificity of the sample examined, one or another approach is preferred. In all these modes of operation, the subwavelength resolution is achieved due to the evanescent waves mediated interaction between the probe and the sample. A good introduction in the field of near-field microscopy and nano-optics can be found in several recent reviews [7],[15]-[19].

The experiments included in this thesis were performed using a near field scanning optical microscope (Nanonics NSOM-100) which is presented in Figure 2. The instrument can be used in both illumination and collection modes of operation in order to obtain simultaneously optical images and the corresponding atomic force microscopy (AFM) topography [20]. The near field scanning optical microscope (NSOM) fully integrates near-field optics with atomic force microscopy and scanned probe microscopy with conventional optical microscopy.

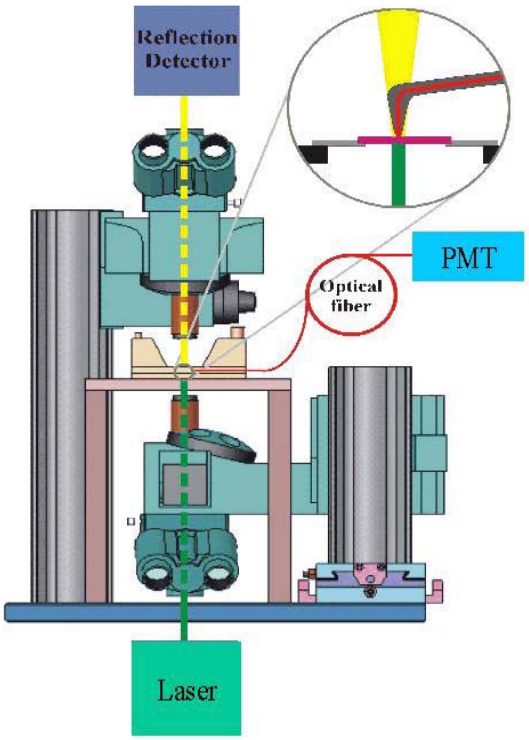

Figure 2: Experimental set-up: NSOM instrument capable of both illumination and collection modes of operation.

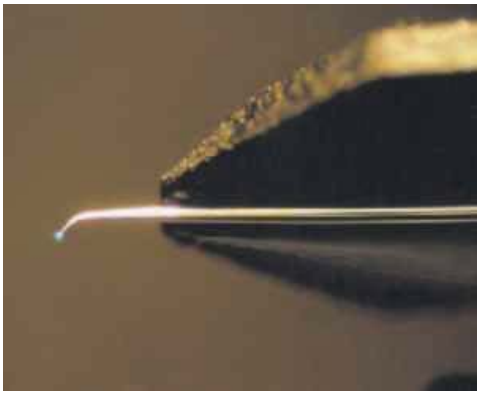

Figure 3: The main element of the NSOM: the Al-coated fused silica fiber tip

The central component in NSOM is a glass optical element (Figure 3) which is constructed from a single mode optical fiber tapered at one of its ends and coated with aluminum [21]-[23]. The cantilevered near-field optical sensor provides the possibility to obtain simultaneous near-field super-resolution optical images as well as high quality topographical images.

Using standard AFM techniques, the tip of the optical fiber can be brought within the near-field of a surface that is to be imaged. As the tip scans the surface of the sample, the light emanating from the tip interacts with the specimen and the scattered light can then be detected in the far field using a avalanche photodiode (APD). This is so called illumination mode. Light that is coupled to the fiber is emanated only from the very end of the taper, through an aperture of 50-200nm in diameter, resulting in maximal fluency at the surface of the sample [26]. The lack of out-of-focus light is a major difference between NSOM and lens based optical scanning techniques such as confocal microscopy.

As an alternative to the illumination mode, one can use the so-called collection mode where the entire specimen to be imaged can be excited by either a laser or a white

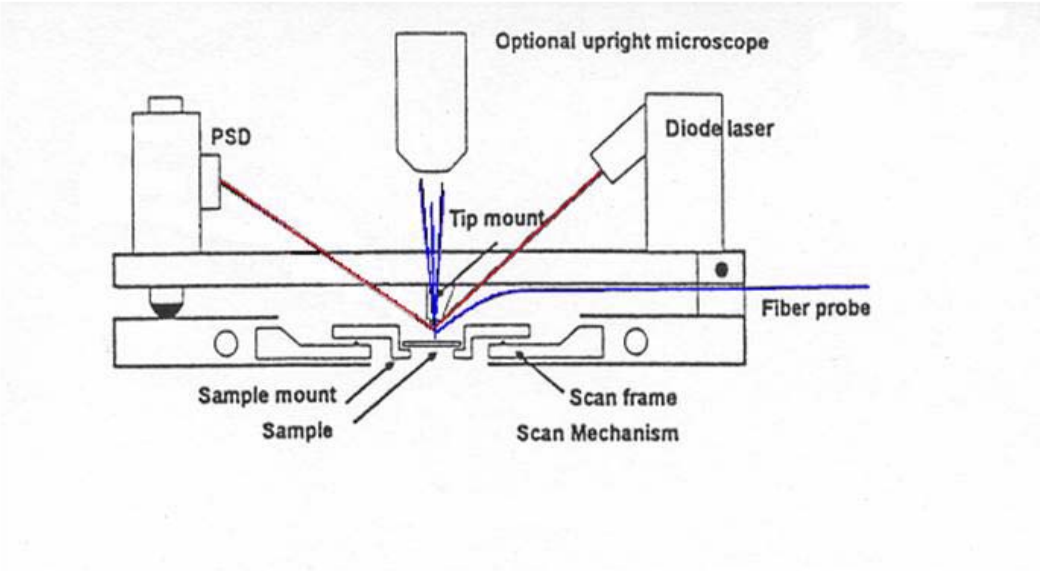

Figure 4: The shear-force feedback mechanism used as a scanning technique is based on collecting the reflection of a laser beam onto a position sensitive detector (PSD). The probe is dithered vertically at its resonance frequency. The PSD signal is feed into a lock in amplifier locked at the tip's resonance frequency. The tip's amplitude of vibration determined by the lock in amplifier is then kept constant by a vertical adjustment of the sample. This provides constant tip-sample separation while the probe is scanned along the sample.

flash lamp. The optical probe is then used as a collection device, capturing the scattered light on the sample, which then can be detected using a photomultiplier (PMT) or other low-light detector. Collection mode also provides a low level of out-of-focus light because the probe only detects light from an extremely small surrounding area.

A shear-force feedback mechanism is used to maintain constant tip height over the sample throughout the scanning [24],[25]. The fiber tip is dithered vertically as it scans the surface to be imaged. Constant tip-sample separation is achieved by the vertical adjustment of the sample to maintain a constant amplitude vibration of the tip. As illustrated in Figure 4, a laser diode is focused on the tip of the fiber and is reflected onto a photo detector. As the tip follows the surface of the sample, the laser diode's reflection changes accordingly, mapping the sample's topography.

The appealing characteristics of the NSOM such as the sub-wavelenght resolution (presented in Section 1.2 and Section 1.3) as well as the simultaneous acquisition of the 3D topography and the optical signal image (illustrated in the present section) make this technique suitable for a large number of applications.

1.4 Imaging applications using NSOM

Probably the most common application of NSOM is the near-field imaging. In particular, the ability to obtain extremely high-resolution images without the requirement of an elaborate sample preparation and without the extremely damaging effects associated with the electron microscopy makes NSOM particularly appealing for the study of biological samples.

1.4.1 NSOM - imaging modalities

As already mentioned in Section 1.3, the near-field scanning optical microscope used for the present studies fully integrates optical microscopy, confocal microscopy, atomic force microscopy and near-field optics for a better topographical and optical resolution. These capabilities are illustrated in the schematic diagram shown in Figure 5. As can be seen, the design of the instrument also provides the possibility of operation in both illumination and collection modes suggested in Figures 1.

In the following, we will exemplify the capabilities of this NSOM operating in illumination and collection modes. The instrument spatial resolution and its light detection efficiency will be demonstrated in different imaging situations involving biological cells and various dielectric structures. In another example, near-field fluorescence imaging will be illustrated as a possibility for retrieving information about the proteins distribution on tumor cell membrane. Using this technique, both surface and subsurface melanoma cell proteins have been identified.

As a first example we present in Figure 6 a bright-field, optical microscopy image of A375 human melanoma cells. As indicated by the square in Figure 6, the $50nm$ aperture NSOM tip was positioned at the center of the field of view which size is approximately 300x300μm. The AFM scanning techniques described above were then used to zoom in the optical image and to obtain a much better resolved image, which is shown in Figure 7.

In the collection mode of operation, light transmitted or reflected by the sample is coupled to the near-field optical force sensor. The tip also acts, like in the previous

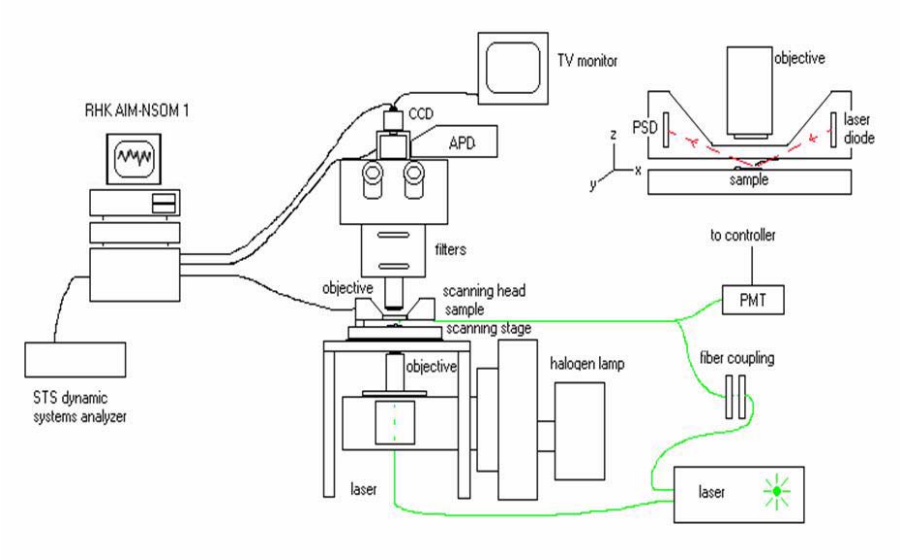

Figure 5: Experimental set-up: NSOM instrument integrating optical microscopy, confocal microscopy, atomic force microscopy with near-field optics. The design of the instrument also provides the possibility of operation in both illumination and collection modes. In illumination mode of operation, an Ar+ Ion Laser ($488nm$) beam is coupled to one end of the fiber tip and the radiation is emanated from the other end, tapered down to diameter of $50 - 200nm$. The light interactes with the medium and the scattered field is detected in far-field by an avalanche photodiode (APD). In collection mode of operation, the sample is illuminated by the Ar+ Ion Laser beam and the transmitted field is coupled to the near-field porbe while the scattered light is detected by a PMT operating in photon counting mode.

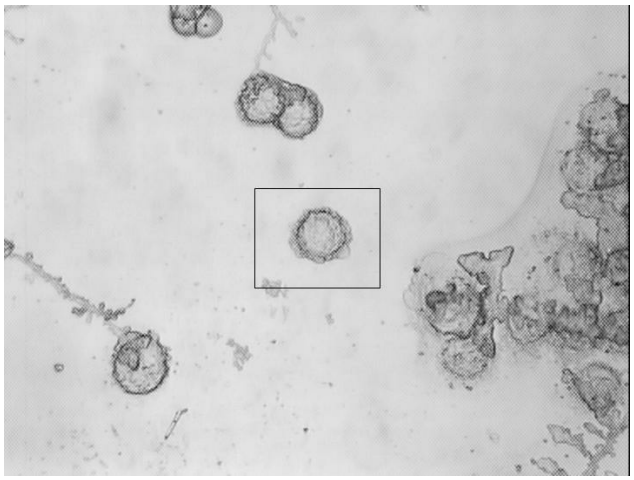

Figure 6: Optical image of the A375 human melanoma cells. The field of view represents approximative 300x300μm.

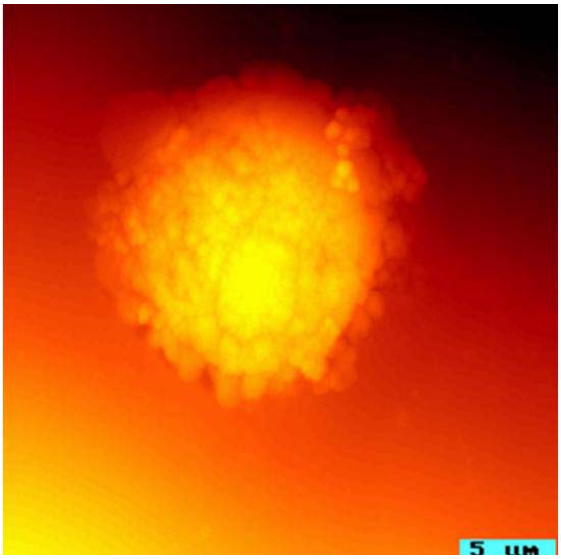

Figure 7: AFM image of the a center cell of the optical image presented in Figure 6.

example, as an AFM probe. Examples of both topographical and near-field optical images obtained in the collection-transmision geometry are shown in Figures 8. The sample examined was a slab of polystyrene spheres with a diameter of $356nm$ which were illuminated in transmission by an Ar+ Ion Laser ($\lambda = 488nm$). The scattered light is detected by a PMT operating in photon counting mode. The optical image resembles a typical speckle pattern. Different characteristics of this intensity distribution will be discussed in detail in Chapter 2 and Chapter 3.

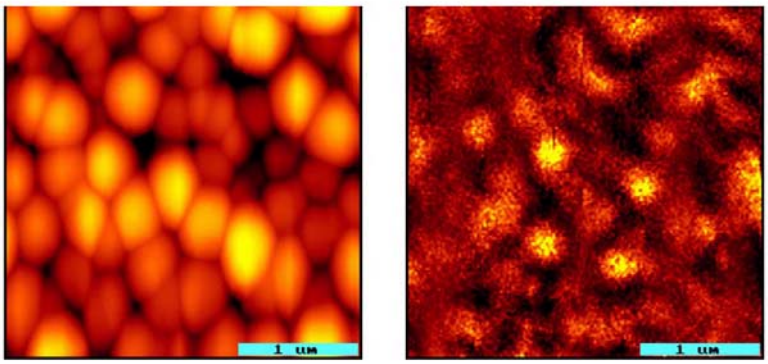

Figure 8: a) Topography of slabs containing polystyrene spheres; b) Near-field intensity distribution collected over the same area in transmission-collection mode of operation.

As mentioned before, the NSOM operation can also be in an illumination mode. In this case, as the tip scans the surface of the sample, the light emanating from the tip aperture interacts with the specimen. The radiation is coupled onto the medium and is

then reemitted and detected in the far-field. Simultaneously with the detection of the optical signal, the surface heights distribution is also recorded.

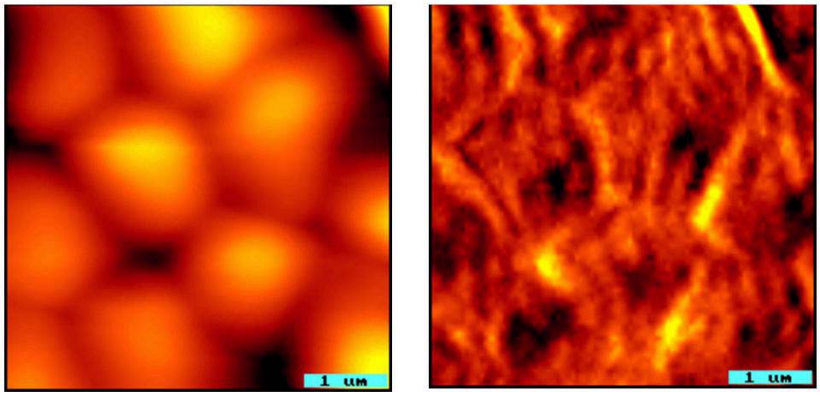

Figure 9: a) Topography of monolayer containing silica spheres; b) Near-field intensity distribution collected over the same area.

To illustrate this, an example of both topographical and near-field optical images for a monolayer containing silica spheres of $1500nm$ diameter is presented in Figures 9. The radiation is provided by a green laser ($\lambda = 532nm$) coupled to the fiber tip. The scattered light is collected by the microscope objective and then detected by an APD as shown in the schematic of Figure 5. In this situation, when the $100nm$ aperture tip scans the sample, the coupling of radiation onto the medium depends of the local slope of the physical dielectric interface. This, together with possible cross-talking between the silica spheres, induces a collective response of the dielectric microparticles. For specific size and arrangement of certain dielectric spheres, the collective modes should depend on

the relative position of the tip with respect to the sphere surface. These collective modes of the dielectric structure can explain the intensity variations and the presence of regular fringes surrounding the microspheres in Figure 9b.

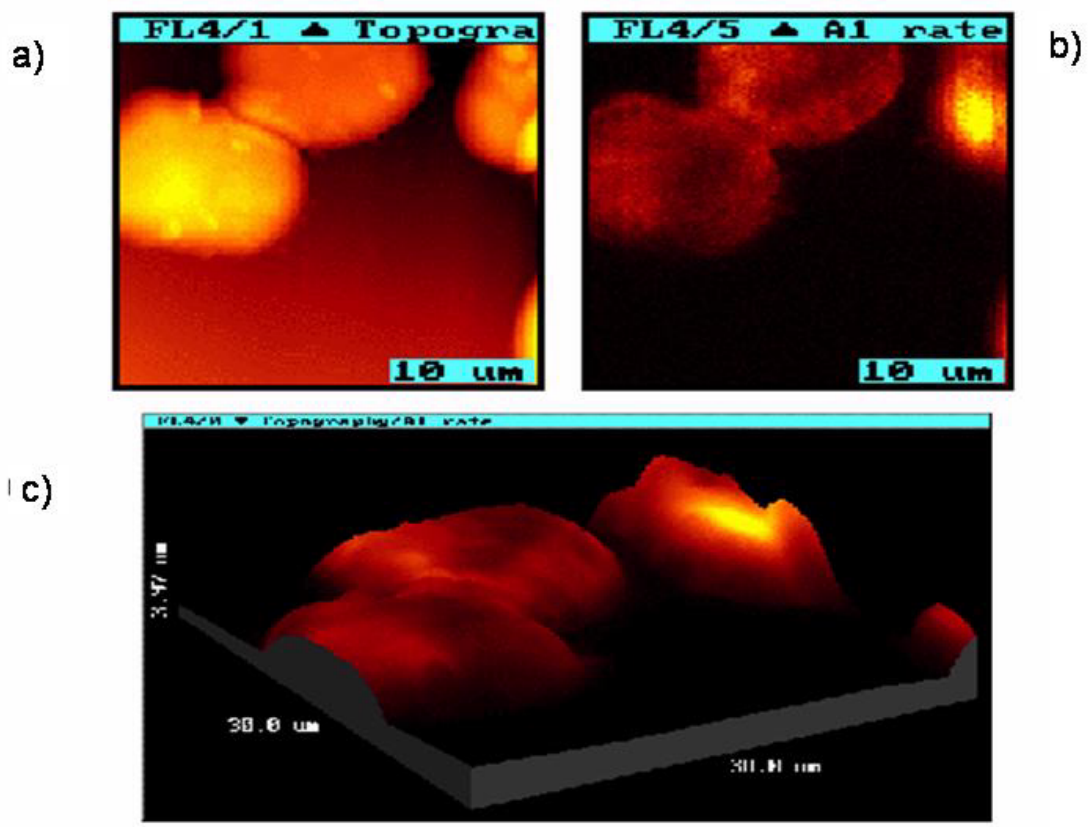

Figure 10: A375 Melonoma Cells treated with Lipid Membrane Tracer (DIO). a) AFM topography. b) Near-field fluorescence image. c) Fluorescence signal imposed as a color value to the topography.

A particular case of the illumination mode of operation is the near-field fluorescence imaging. This is illustrated in Figures 10 where, using appropriate detection filtering techniques for fluorescence collection, the near-field fluorescence image can be obtained simultaneously with the AFM topography. The example illustrated in Figure 10b presents

a biological cell incubated with specific fluorescent dye called DIO. The dye is excited by $488nm$ line of the Ar+ Ion Laser and the $535nm$ fluorescence is collected by the APD after filtering the excitation beam. Because the fluorescence signal and the topography of the cell are collected simultaneously, one can visualize the exact distribution of the fluorescence on the sample surface. We present in Figure 10c an example of the near-field fluorescence signal superimposed as a color value to the three-dimensional topographical image. This turns out to be a very unique capability of the NSOM operation because it offers the possibility to determine the spatial distribution of emission with high spatial resolution.

The traditional approach to study cells fluorescence has been confocal microscopy. However, being based on the propagation of optical waves, the resolution, in this case, is limited by the diffraction of light. The resolution of NSOM techniques, on the other hand, is limited only by the volume interaction between the tip and the sample. Therefore, they provide the possibility to obtain highly resolved AFM images as well as fluorescence near-field super-resolution optical images. A comparison between the confocal images and the NSOM ones is presented in Figures 11 for the topography and in Figures 12 for the optical images. One can notice that the peripheral micro-extensions (microspikes) shown in Figures 11 have extremely small features compared with the cell's dimensions, measuring approximately $500nm$ wide and $300nm$ thick, and they can not be resolved using confocal microscopy, as illustrated in Figure 11a. However, using a sub-wavelength probe of $50nm$, a resolution better than $100nm$ is easily achieved for the AFM topographies and a $180nm$ resolution for the corresponding optical images. The microspikes are very

well resolved (Figure 11b) and the technique also offers significant advances in detecting localized proteins (Figure 12b).

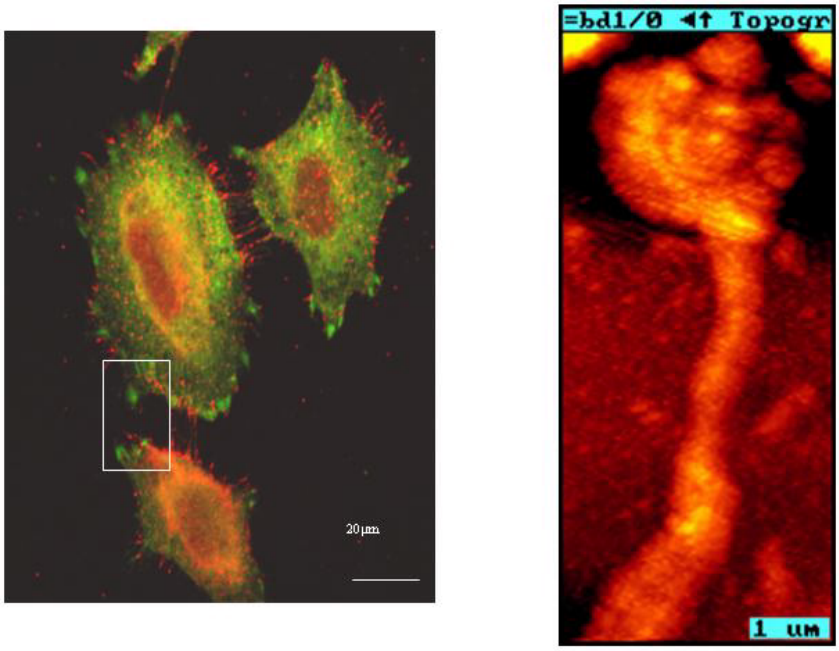

Figure 11: Comparison between confocal microscopy and AFM. a) confocal image of melanoma cells immunolabeled for NF2 and ErB2 (green and red, respectively). Microspikes extend between adjacent cells as indicated. b) AFM topographical image of a microspike extending from a globular domain on the surface of a melanoma cell.

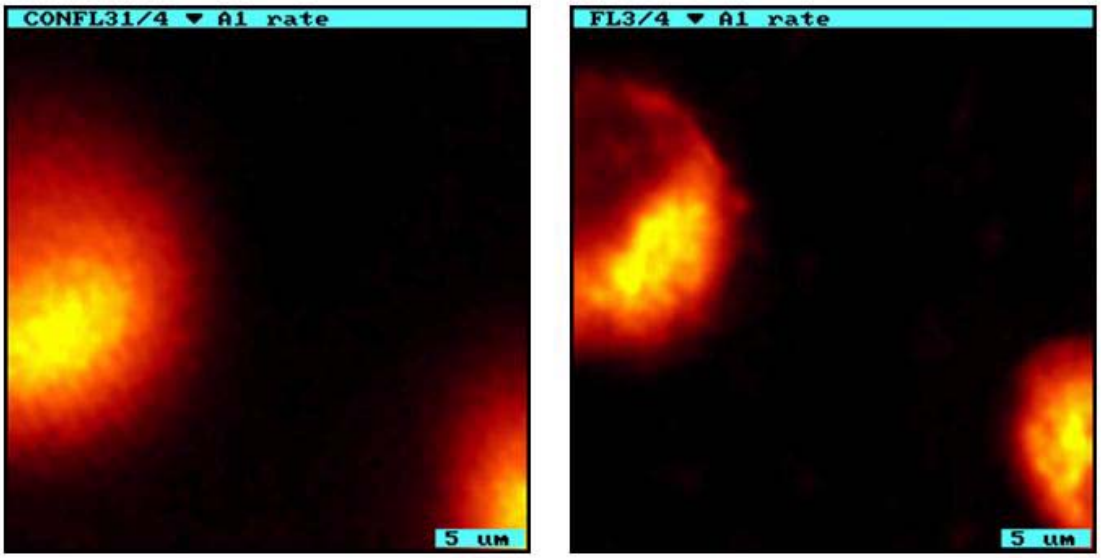

Figure 12: Comparison between the confocal fluorescence imaging (a) and the NSOM fluorescence imaging (b) for A375 cells treated with DIO.

1.4.2 Near-field fluorescence imaging of human melanoma cells

Based on the capabilities outlined in the preceding section, near-field scanning optical microscopy (NSOM) proved a viable approach for studying of different biological processes. NSOM provides high-resolution optical images without elaborate sample preparation and without damaging the sample [27]-[30] and in the following I will present how this technique helps understanding proteins interactions which are involved in cellular processes [31]-[33].

In the previous section, it was illustrated how NSOM can detect localized proteins on A375 human melanoma cells. Using similar NSOM capabilities, we have also imaged the distribution of two proteins on the melanoma cells: CD54 (ICAM-1) and NF2. The example is interesting because it demonstrates the identification capability of both surface (CD54) and subsurface (NF2) melanoma cell proteins.

CD54, also known as ICAM-1 or intercellular adhesion molecule 1, is an adhesion molecule identified on the surface of various tumor cells. It plays various roles in mediating the body's immune response to tumor growth and metastasis. Studies have identified correlations between CD54 and cytotoxicity [34], adhesion of T-cells to tumor cells [35], natural killer cell lysis and its relation to tumor necrosis factor (TNF) [36]. It has been suggested that tumor cells' weak surface ICAM expression may provide a means by which melanomas remain undetected by the immune system [37]. The study of CD54 distribution and function, therefore, may be especially pertinent to determining why the body's immune system is ineffective at destroying soluble tumors.

Neurofibromatosis-2 (NF2) is an autosomal dominant disease caused by alterations in the NF2 gene [38]-[40]. The disorder is characterized by the formation of bilateral vestibular Schwannomas and cerebral meningiomas [41]. These tumors are believed to form due to major structural impairments of the gene's product, Schwannomin (merlin) [42]-[44]. NF2 has been identified within the substructure of melanoma cells. It is believed that the NF2 gene in such cells is mutated in a similar way as that of malfunctioning Schwann cells. The tumors produced by melanoma cells are malignant, whereas the tumors produced by Schwann cells are benign. By studying NF2, scientists hope to understand not only the growth signaling pathways of melanoma cells as well as their lack of contact growth inhibition, but also the difference between merlin produced by impaired Schwann cells and the merlin produced by melanoma cells.

Materials and Methods. A375 human melanoma cells were cultured in RPMI-1640 supplemented with 10% fetal bovine serum, penicillin and streptomycin. Subconfluent cultures were harvested with trypsin EDTA washed with PBS without calcium and magnesium and the concentration adjusted appropriately for various experiments.

Harvested A375 cells (approximately 2 x 105 cells/sample) were grown on $\frac{3}{4}$" glass cover slips for 24 hours. Cells were fixed with paraformaldehyde and incubated with phosphate buffered saline (PBS). They were then reacted with rabbit anti-human NF2 and with Oregon green conjugated goat anti-rabbit IgG.

Samples conjugated with the fluorophore Oregon green were excited by a $488nm$ line of an Ar+ Ion laser. The excitation beam was coupled to the NSOM fiber probe illu-

minating the sample and the $535nm$ fluorescence emissions were collected by an avalanche photodiode (APD). A longpass $515nm$ filter was used to block the $488nm$ excitation beam.

Protein distribution on the surface of human melanoma cells. Figure 13a shows an optical image of human melanoma cells labeled with antibody against CD54 and immunolabeled with Oregon green conjugated secondary antibody. A $50nm$ aperture optical cantilever was used to scan the central cell, as indicated in Figure 13a. Figure 13b shows a three dimensional representation of the acquired topography and the detected fluorescence signal. Because of the high spatial resolution available we were able to detect small details of antigen's distribution across the cell membrane.

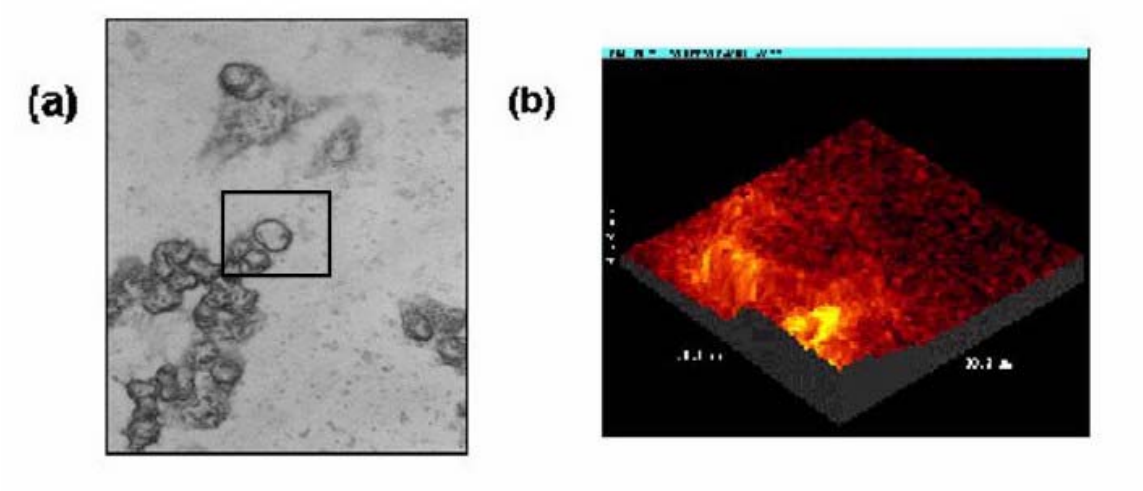

Figure 13: A 375 human melanoma cells labeled with antibody against CD54 and immunolabeled with Oregon green conjugated secondary antibody. (a)optical image; (b) CD54 distribution on the surface of the central cell of the optical image. Fluorescence intensity represented as a color-scale imprinted upon the three-dimensional topography image.

The fluorescence image obtained is consistent with the fact that CD54 is an adhesion molecule found on the surface of various melanoma cells. It is worth mentioning that such adhesion molecules are not expected to be distributed uniformly across the surface of the cell as in the case of the lipid tracer presented in Figure 10b. It is evident in Figure 13b that the fluorescence distributed non uniformly and it concentrated along the edges of the cell. A comparison of NSOM images with previously obtained confocal images further validate the results.

Protein distribution on the sub-surface of human melanoma cells. While the first two imaging cases illustrated in Figure 10c and in Figure 13b detected fluorescence originating on the surface of the cell membrane, NF2 fluorescence is emitted beneath the membrane surface. In Figure 14 we present the image taken of NF2 distribution encompassed the entire cell body. Minimal fluorescence signal was detected due to the small aperture. Moreover, the radiation exiting the aperture is attenuated away from the tip before reaching the NF2 location, beneath the cell surface. The bright spots indicating elevated light intensity are most likely representative of high NF2 concentrations surrounding focal adhesions.

In conclusion, this section demonstrates some of the NSOM capabilities in cell biology. High resolution fluorescence images and 3D topographical data were simultaneously acquired for various immunolabeled proteins on the surface and subsurface of human melanoma cells. The results presented here illustrate the flexibility of NSOM techniques in retrieving information regarding cell structure and protein distribution.

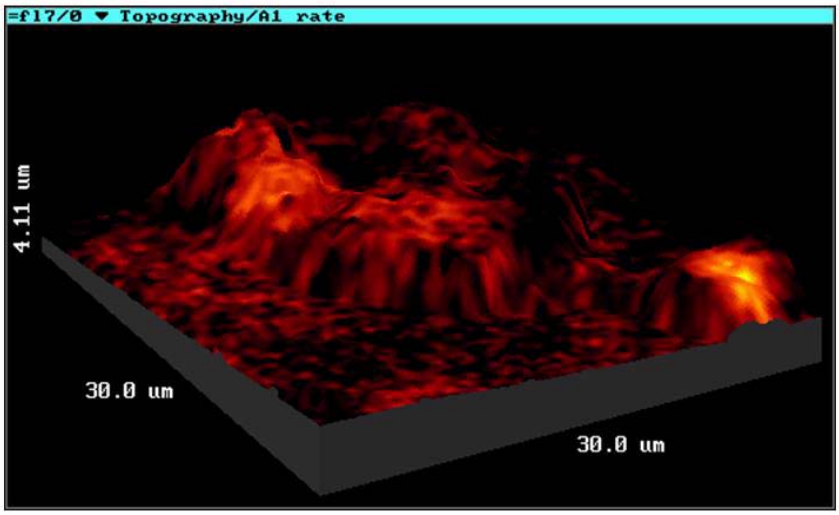

Figure 14: NF2 distribution on an A375 human melanoma cell. Fluorescence intensity represented as a color-scale imprinted upon the three-dimensional topography image

As we have seen, the capability to collect fluorescent radiation at low light levels and with high spatial resolution allow visualizing protein distribution on the surface and subsurface of optically inhomogeneous structures such as biological cells.

These proven capabilities of an NSOM instrumentation will be further used in the next sections to study in detail the coherence characteristics of radiation emitted by randomly inhomogeneous media. The experimental approaches specific to near-field optics will be crucial in determining the properties of the detected fields and will permit exploring subtle effects such as discriminating between the surface and subsurface effects.

CHAPTER TWO: GAUSSIAN STATISTICS OF LIGHT FLUCTUATIONS IN THE NEAR-FIELD OF A RANDOM MEDIA

The interaction between optical waves and random inhomogeneous media has been systematically investigated and it is now well understood that the familiar appearance of speckle patterns can be described in terms of Gaussian or non-Gaussian statistics of light fluctuations. Far-field intensity variations have been studied in detail [2],[59]-[61]. However, as we already mentioned in Chapter 1, the presence of the evanescent waves in the near-field of random media may affect the statistical properties of optical fields. This determines new aspects of the near-field coherence phenomena which will be discuss in this chapter. Near-field scanning optical techniques will be employed to study experimentally the specific effects of field correlations in the vicinity of interfaces.

When light propagates through a medium with microscale fluctuations of the refractive index, the multiple scattering events randomize the direction and the phase of the optical radiation. The multiple scattering events in the bulk of the medium and on its surface may be responsible for a uniform phase distribution of the transmitted field. This, together with the fact that the amplitudes and the phases of the field originating from a large number of elementary scattering centers N are statistically independent random

variables, allows one to consider that the real and imaginary parts of the complex scattered field obey circular Gaussian statistics. Consequently, the amplitude of the resultant field has a Rayleigh distribution and the corresponding intensity is exponentially distributed.

This chapter describes the transmission-collection configuration in which near-field scanning optical microscope (NSOM) can be used to study various aspects of the field coherence properties in the close vicinity of the random media. These characteristics of radiation emitted from or transmitted through a highly inhomogeneous media will be then discussed in detail in Chapter 2 to Chapter 4. A brief description of the random media under the study is presented in this chapter along with experimental evidence of evanescent waves contribution to the total detected signal. The analysis of intensity fluctuations will demonstrate that the radiation properties can be described in the regime of Gaussian statistics.

2.1 Experimental situations

Situations where the intensity variations in the near-field of highly inhomogeneous media satisfy the requirements of circular Gaussian statistics can be encountered experimentally when the media is globally excited in so-called transmission-collection geometry. In this configuration which is illustrated in Figure 15, radiation from a light source propagates through a random medium and is collected at the surface by an NSOM. In practice, an Ar+ Ion Laser ($\lambda = 488nm$) or a white LED (for the spectral measurements) are used to illuminate the random medium and the transmitted field is coupled to the cantilevered near-field optical force sensor while the tip is scanned along the sample. The scattered light is detected by a PMT operating in photon counting mode. The near-field scanning

optical microscope (Nanonics NSOM-100) allows obtaining simultaneously the optical images and the corresponding AFM topography as explained in the previous section.

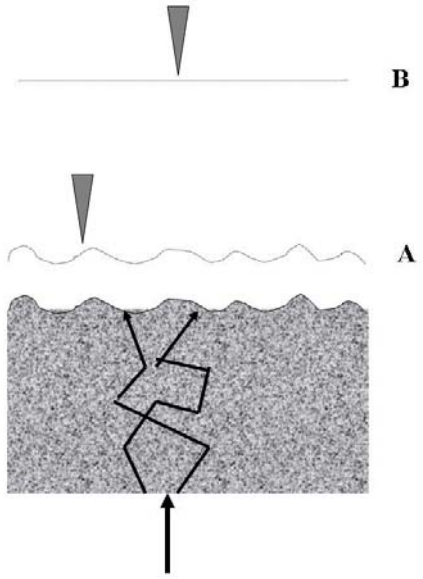

Figure 15: Transmission-collection experimental configuration. The NSOM probe can be used to scan in both constant distance (A) and constant height (B) modes.

In the following, we will refer as "near-field" to images collected at distances z smaller than the wavelength, and as "far-field" for those distances z of the order of 5-20 wavelengths from the interface. The Al-coated fused silica fiber tip with an aperture of $50-200nm$ provides the possibility to scan in constant distance (for the near-field images) or in constant height mode (for the far-field images).

We measured the first and second-order statistical properties of optical fields near the surface of various random, highly scattering media which were illuminated in a transmission geometry. Our results refer to physical situations where media with strong volume randomness are bounded by relatively smooth surface with slowly varying interfaces.

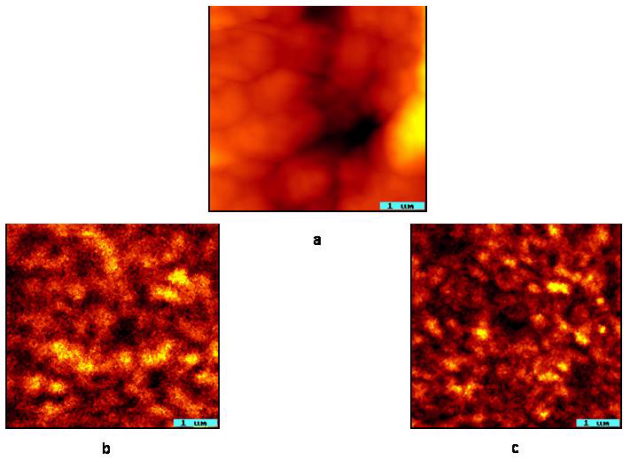

Figure 16: (a) Topography of compact slabs made of calcium carbonate and kaolin microparticles; the r.m.s roughness is $200nm$. (b) Far-field intensity distribution collected over the same area at $z = 5000nm$ away from the interface. (c) Near-field intensity distribution collected over the same area at $z = 45nm$away from the interface.

The data were collected on three different media: (i) compact slabs made of calcium carbonate and kaolin microparticles (average diameter of $400nm$ and average refractive index of 1.46), (ii) slabs containing polystyrene spheres of $356nm$ diameter, and (iii) VYCOR porous glass samples with 28% void volume and $4nm$ average pore size. Their scattering properties are characterized by the correlation length of the refractive index fluctuation and by the r.m.s height of the surface which typically range between 100 and $250nm$ for the microparticles slabs and between 13 and $50nm$ for the VYCOR glass. Typical topographical images and their corresponding far- and near-field intensity distributions are presented in Figures 16, Figures 17 and Figures 18 for the compact slabs made of calcium carbonate and kaolin microparticles, for the slab containing polystyrene spheres and for the VYCOR glass sample, respectively. The images presented here are

obtained using a $150nm$ aperture tip in the case of the slabs and a $200nm$ aperture tip for the VYCOR glass sample.

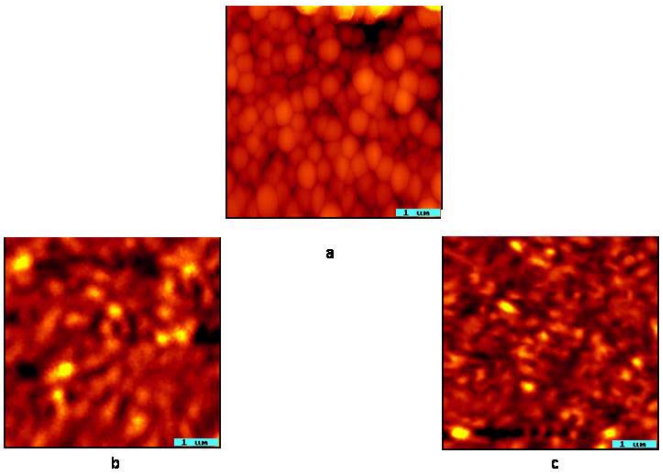

Figure 17: (a) Topography of slabs containing polystyrene spheres; the r.m.s roughness is $208nm$. (b) Far-field intensity distribution collected over the same area at $z = 5000nm$ away from the interface. (c) Near-field intensity distribution collected over the same area at $z = 45nm$ away from the interface.

The AFM images give information about the sample morphology. Statistical quantities like r.m.s standard deviation of the height fluctuations, local slope standard deviation and lateral correlation of the surface heights can then be used to characterize the sample topography. The optical images, on the other hand, are determined by the values of the optical intensities and permit estimating the coherence properties of optical near-fields. The following sections will describe the analysis of first and second-order statistical properties of the fields in the vicinity of random media. Two main characteristics of the optical near-fields close to the random medium are the contribution of evanescent waves

and the specific probability density function of intensity fluctuations. They determine all the statistical properties and will be discussed in Section 2.2. and Section 2.3.

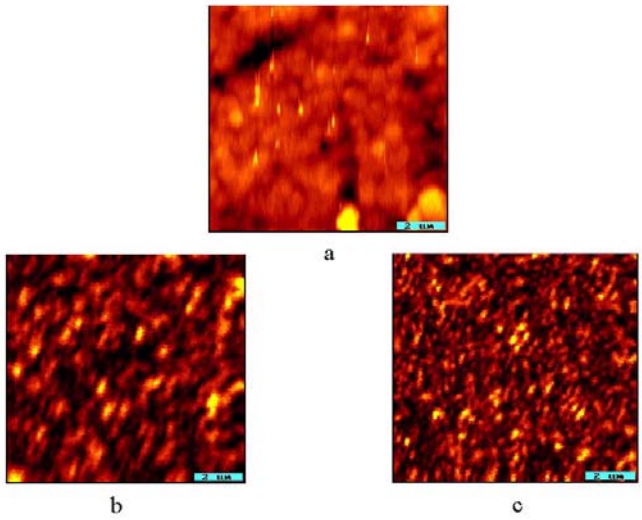

Figure 18: (a) Topography of VYCOR glass sample; the r.m.s roughness is $13.4nm$. (b) Far-field intensity distribution collected over the same area at $z = 5000nm$ away from the interface. (c) Near-field intensity distribution collected over the same area at $z = 20nm$ away from the interface.

2.2 Evanescent waves contribution

As shown in Figure 15, the optical radiation is randomized throughout the bulk of the medium and the directions of the waves reaching the surface together with the topographical characteristics of the surface determine both propagating and evanescent waves in the near-field of the medium. In the close vicinity of the surface of such highly random media, the NSOM probe collects both the homogeneous and inhomogeneous components of the emitted field. When the intensity recorded is averaged over scanning areas situated at increasing distances z from the surface the average intensity manifests a negative

exponential dependence on z, indicating that the detected signal contains a significant contribution of inhomogeneous components. As expected, this contribution vanishes at distances z larger than the wavelength of light, where only the homogeneous components are contributing. For the compact slabs sample made of calcium carbonate and kaolin microparticles, the ratio $\langle I_{NF}\rangle/\langle I_{FF}\rangle$ between the near- and far-field average intensities is plotted in Figure 19 as function of the distance z. The experimental data shown in Figure 19 can be quantitatively described by a model which will be presented in detail in Chapter 3 and which will fully account for the contribution of evanescent waves.

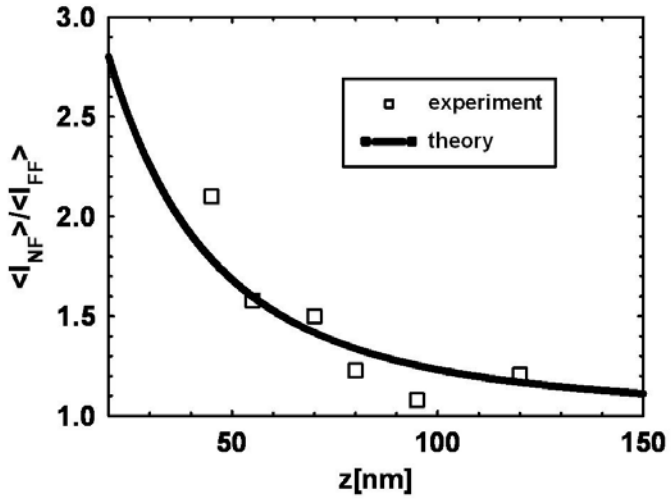

Figure 19: Typical example of average intenstity as function of distance z. The experimental ratio of near- and far-field intensity (dots) are fitted with a negative exponential function as explained in Chapter 3.

2.3 Probability density function of intensity fluctuations

When examining the experimental data, we note that the spatial distribution of the detected intensity resembles the typical intensity variations present in a classical speckle

pattern. In a given observation point, the field is a superposition of large number of contributions originating from different locations within the bulk of the random medium and one can consider that the amplitude and the phase of the elementary phasors satisfy the requirements of circular Gaussian statistics. This assumption is confirmed by the first-order statistics of intensities measured in both near- and far-field.

In any real experiment, the measured first-order statistics of speckle field is affected by noise. In order to minimize this influence, in our experiments we adjusted the intensity of the radiation incident on the random medium such that the average intensity of the near- and far-field speckle patterns were about the same. Typical results of near- and far-field measurements are presented in Figure 20 where the measured intensity probability density function $p(I)$ multiplied by the average intensity $\langle I \rangle$ is plotted in a logaritmic scale as a function of the normalized point intensity $I/\langle I \rangle$. As can be seen, the measured intensity probability density function $p(I)$ obeys a negative exponential dependence for both near- and far-field. Consequently, the optical contrast, $\sqrt{\left\langle \langle I^2 \rangle - \langle I \rangle^2 \right\rangle} / \langle I \rangle$ is close to 1 in all situations. We emphasize that the first-order statistics were determined for radiation collected above the same region of the surface, the distance z being the only variable parameter. The data presented in Figure 20 are collected on VYCOR glass sample with r.m.s roughness of $13nm$ but the same behavior of intensity distribution was also obtained for the other samples with the r.m.s. fluctuations of the surface height ranging between $\lambda/40$ and $\lambda/2$. The experimental data clearly shows that the single-point statistical properties are the same in the both the near- and far-field speckle patterns.

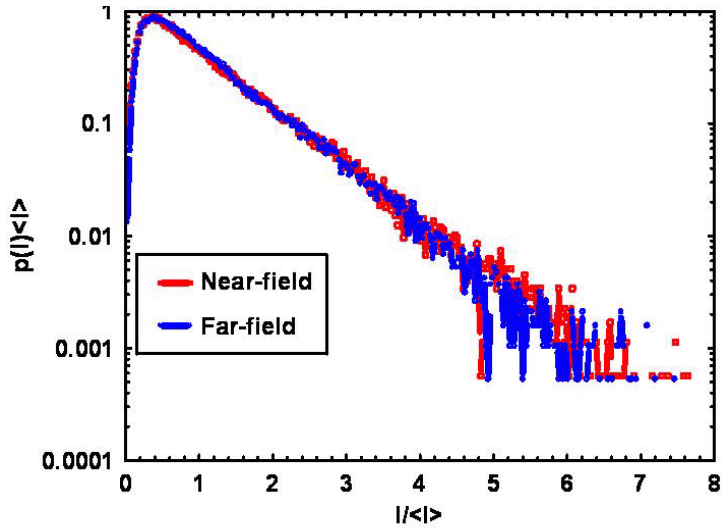

Figure 20: Normalized intensity probability density function measured in the near-field ($z = 20nm$) and in the far-field ($z = 5000nm$) of the VYCOR glass sample.

The regime of near-field Gaussian statistics is achieved due to the strong multiple scattering which uniformly distributes the phases of the elementary scattering centers and increases the number of field contributions in any examined point, irrespective of the distances z from the physical interface and also, irrespective of the values of the r.m.s. fluctuations of surface height.

This observation permits examining further the spatial coherence properties in the vicinity of such interfaces by using just intensity measurements. A quite different statistical regime of intensity fluctuations is obtained in the so-called NSOM illumination mode and will be discussed in detail in Chapter 5.

CHAPTER THREE: SPATIAL COHERENCE PROPERTIES IN THE VICINITY OF INTERFACES

As demonstrated in the previous chapter, the properties of near-field radiation emerging from a randomly inhomogeneous medium can be described in terms of Gaussian statistics of light fluctuations. Moreover, the radiation originating from random media is commonly regarded as being spatially incoherent. A classical example of such incoherent source is a thermal one.

The optical coherence theory predicts that the quasi-homogeneous Lambertian sources of radiation are not completely spatially incoherent; at a given optical frequency ω, the field correlates over regions whose spatial dimensions are of the order of the wavelength $\lambda = 2\pi c/\omega$ [5]. It is important to emphasize that this fundamental result has been obtained by neglecting the contribution of short-range evanescent waves and it has been successful in describing the far-field properties of thermal emission.

Recent advances in experimental capabilities and an increasing interest in nanoscale phenomena have raised new questions regarding the emission of optical radiation and, in general, the coherence properties in the near-field [45]-[49]. Very recently, it has been suggested that the spatial coherence length of the field close to the surface of a thermal source

may be either much larger or much smaller than the wavelength of the light depending on the dominant contribution to the cross-spectral density tensor [46],[50].

This chapter brings the first experimental evidence that, at distances smaller than the wavelength of light, contrary to the predictions of conventional coherence theory, the coherence length can be smaller than the wavelength. Moreover, it will be shown that the coherence length of the emitted field in the near-field depends on both the detailed structure of the source and the distance from the interface. The present chapter also demonstrates that, at several wavelengths away from a surface, the spatial coherence properties of the field can be used to determine the statistical properties of an inhomogeneous interface. All these results are obtained using the NSOM capabilities outlined in Chapter 1, namely the superresolution and the simultaneous acquisition of the 3D topography together with the optical image. The data analysis is based on the two main characteristics of the optical near-fields close to the interface of a random medium which were discussed in Chapter 2, namely the exponentially decaying contribution of evanescent waves and the specifics of Gaussian statistics regime of optical near-fields.

3.1 Spatial coherence properties as function of distance from the interface

A description of the field distribution can be developed if the surface of the random medium is considered equivalent to a homogeneous, planar, statistically stationary source of optical radiation [5]. Using the capabilities of near-field scanning techniques which were illustrated in Chapter 1, it is also possible to measure coherence effects in the near-field of the highly inhomogeneous media which are known to produce significant field fluctuations and a radiant intensity typical to incoherent sources. It is also important to realize that,

due to the small dimensions of both the scanning area and the probe, the surface of the sample can be considered to be an infinitely extended source of optical radiation.

3.1.1 Cross-spectral density near the surface of a homogeneous, planar, statistically stationary source of optical radiation

An homogeneous, planar, statistically stationary source of optical radiation [5], located at $z = 0$, is characterized by a cross-spectral density function [51]

$$W^{(0)}(\boldsymbol{\rho}_1, \boldsymbol{\rho}_2, \omega) = F^{(0)}(\boldsymbol{\rho}_2 - \boldsymbol{\rho}_1, \omega), \tag{11}$$

where $\boldsymbol{\rho}_1$and $\boldsymbol{\rho}_2$ are two-dimensional position vectors in the plane of the source and ω is the radiation frequency.

The source generates, in the half space $z > 0$, a field with the cross-spectral density function given by [51]:

$$W(\mathbf{r}_1, \mathbf{r}_2, \omega) = k^2 \iint_{-\infty}^{\infty} \tilde{F}(ks_x, ks_y, \omega) e^{ik(\mathbf{s}\mathbf{r}_1 - \mathbf{s}^*\mathbf{r}_2)} ds_x ds_y, \tag{12}$$

where $\tilde{F}(ks_x, ks_y, \omega)$ is the two dimensional Fourier transform of cross spectral density at $z = 0$, $F^{(0)}(\boldsymbol{\rho}_1 - \boldsymbol{\rho}_2, \omega)$.

In general, one can decompose the cross spectral density function in low- and high-frequency components

$$W(\delta x, \delta y, z, \omega) = W_{\mathrm{hom}}(\delta x, \delta y, \omega) + W_{ev}(\delta x, \delta y, z, \omega) \tag{13}$$

where the homogeneous component of the cross-spectral density function is:

$$W_{\hom}(\delta x, \delta y, \omega) = k^2 \iint_{s_x^2+s_y^2 \leqslant 1} \tilde{F}(ks_x, ks_y, \omega) e^{ik(s_x \delta x + s_y \delta y)} ds_x ds_y \tag{14}$$

and the inhomogeneous one is evaluated like:

$$W_{ev}(\delta x, \delta y, z, \omega) = k^2 \iint_{s_x^2+s_y^2 > 1} \tilde{F}(ks_x, ks_y, \omega) e^{(ik(s_x \delta x + s_y \delta y))} e^{(-2kz\sqrt{s_x^2+s_y^2-1})} ds_x ds_y, \tag{15}$$

where $\mathbf{r}_2 - \mathbf{r}_1 = (\delta x, \delta y, 0)$ and $\mathbf{s} = (s_x, s_y, \sqrt{1 - s_x^2 - s_y^2})$. It is worth mentioning that the conventional treatment of the spatial coherence properties of planar sources has been conducted by neglecting the high-frequency components of the cross-spectral density function which are associated with the evanescent field near the surface [51].

As can be seen, the coherence function W is practically determined by the spectral degree of coherence in the source plane at $z = 0$

$$\mu^{(0)}(\boldsymbol{\rho}_2 - \boldsymbol{\rho}_1, \omega) = \frac{F^{(0)}(\boldsymbol{\rho}_2 - \boldsymbol{\rho}_1, \omega)}{S^{(0)}(\omega)}, \tag{16}$$

where $S^{(0)}(\omega) = F^{(0)}(0, \omega)$ is the spectrum of the light in the plane of the source. We consider a Gaussian correlated source with its spectral degree of coherence of the form

$$\mu^{(0)}(\boldsymbol{\rho}_2 - \boldsymbol{\rho}_1, \omega) = \exp(-(\boldsymbol{\rho}_2 - \boldsymbol{\rho}_1)^2/2\sigma^2), \tag{17}$$

where σ is the field correlation length in the plane of the source. Straightforward algebra leads to

$$W_{\hom}(r, \omega) = \pi k^2 \sigma^2 S^{(0)}(\omega) \int_0^1 \rho e^{-\frac{k^2\sigma^2\rho^2}{2}} J_0(k\rho r) d\rho \tag{18}$$

and

$$W_{ev}(r,z,\omega) = \pi k^2 \sigma^2 S^{(0)}(\omega) \int_1^\infty \rho e^{-\frac{k^2\sigma^2\rho^2}{2}} J_0(k\rho r) e^{-2kz\sqrt{\rho^2-1}} d\rho, \tag{19}$$

where $\delta x = r\cos\theta$, $\delta y = r\sin\theta$ and $s_x = \rho\cos\phi$, $s_y = \rho\sin\phi$.

Using the results in Eqs.(13),(18),(19) we calculate the cross-spectral density as a function of the distance z for different values of the field correlation length σ at $z = 0$. In Figure 21, the values of the field coherence length σ_μ defined as the $1/e$ values of the cross spectral density are plotted as a function of distance z from the surface. The calculations are for $\lambda = 488nm$ and account for both homogeneous and inhomogeneous contributions. One can see that the field coherence length increases with the distance z and that larger values of σ_μ are obtained when the field correlation length in the plane of the source σ is increased.

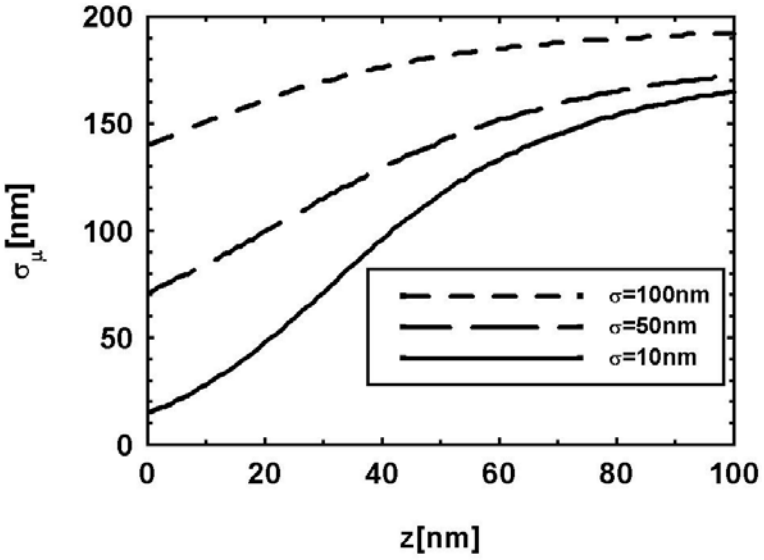

Figure 21: Field coherence length σ_μ as a function of distance z from the surface calculated for different values of the source correlation length σ as indicated. The calculations account for both homogeneous and inhomogeneous contributions.

3.1.2 Spatial coherence at different distances from the interface

From the intensity distributions measured at a given distance z from the interface, the second-order intensity-intensity correlation can be evaluated. As the real and imaginary parts of the complex scattered field have circular Gaussian statistics, standard properties of Gaussian random variables can be used to express the field correlation function in terms of the intensity correlation function [2]. We evaluated numerically the intensity and the field correlation functions and estimated the average radius of the cross section area where the intensity/field correlation decreases at $1/e$ of its maximum. These values were considered as a measure of the speckle size and, respectively, of the field coherence length σ_μ. When estimating the speckle sizes and the field coherence lengths, the experimental data were corrected for the point spread function of the probe.

The results presented in this section correspond to two different media: the compact slabs made of calcium carbonate and kaolin microparticles and the VYCOR porous glass samples. Properties of similar media were described in Section 1 of Chapter 2.

Results of far-field spatial coherence measurements are shown in Figure 22 for the compact slabs and in Figure 23 for the VYCOR sample. Also shown as insets are typical far-field intensity distributions. The data were collected for distances z varying from 1250 to $10000nm$ from the interface. The error bars denote the average over different scanning measurements at the same location across the sample. As can be seen the spatial coherence properties do not depend on the distance z from the surface. This is to be expected from the Equations (13) and (18) when only the contribution from homogeneous components of the field is considered and when the extension of the source is practically infinite.

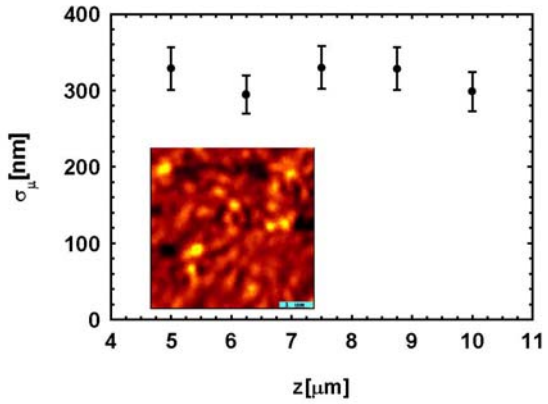

Figure 22: Measured far-field coherence length as a function of the distance z from the surface for the compact slabs made of calcium carbonate and kaolin microparticles. The inset shows a typical far-field intensity distribution.

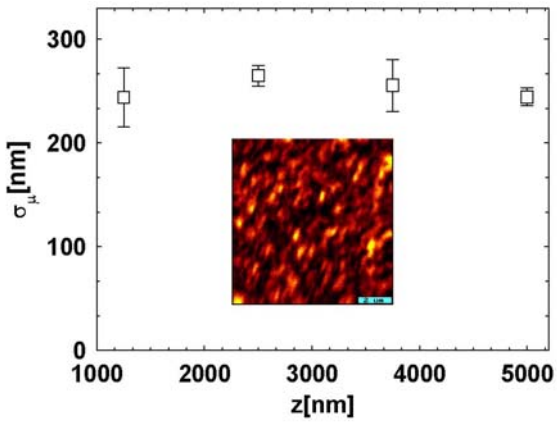

Figure 23: Measured far-field coherence length as a function of the distance z from the surface for VYCOR glass sample. The inset shows a typical far-field intensity distribution.

The experimental values of the coherence length evaluated at a certain distance z vary within less than 8% with respect to the average. Note that classical measurements of spatial coherence properties are performed at much larger distances z where the limited size of the source cannot be ignored. In that case, the size of the coherence area is actually determined by the extent of the source as implied by the Van Cittert-Zernike's theorem [1].

As opposed to the far-field situation, the field coherence length σ_μ measured in the near-field of a highly inhomogeneous medium has a significant dependence on the distance z. In addition, we found that σ_μ is always smaller than the far-field saturation value. This is predicted by our model of optical field radiated by a planar source generating both propagating and evanescent waves. The near-field values of σ_μ plotted as a function of distance z are presented in Figure 24 (compact slabs) and in Figure 25 (VYCOR sample). Also shown with continuous lines are results of the theoretical estimations based on Eqs.(13),(18),(19). For the field correlation length in the plane of the source we used a value of $\sigma = 50nm$ in the case of compact slabs samples and respective $\sigma = 10nm$ in the case of VYCOR glass sample. As can be seen, a fair agreement is obtained with the model described before.

We have also estimated the speckle size near the surface of random media. As expected, the far-field speckle size do not depend on the distance z from the interface while near-field speckle size has a non trivial dependence on z. We present in Figure 26 the near-field speckle size as a function of the distance z from the surface for the VYCOR glass sample. Using the results in Eqs. (13),(18),(19) and standard properties of Gaussian

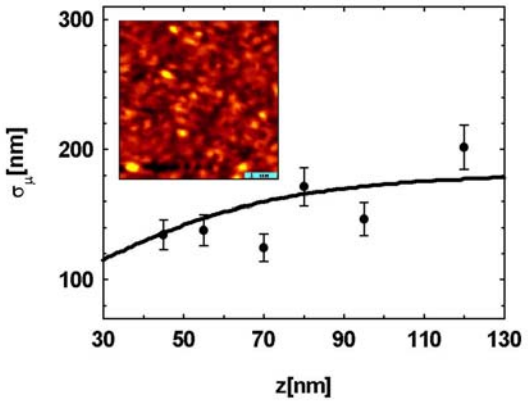

Figure 24: Measured near-field coherence length as a function of the distance z from the surface for the compact slabs made of calcium carbonate and kaolin microparticles. The inset shows a typical near-field intensity distribution.

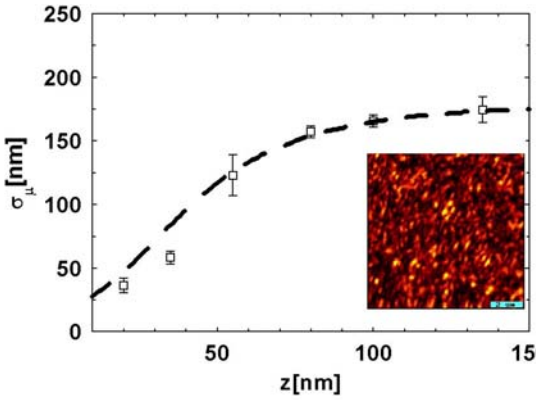

Figure 25: Measured near-field coherence length as a function of the distance z from the surface for VYCOR glass sample. The inset shows a typical near-field intensity distribution.

random variables we have calculated the intensity-intensity correlation function and the corresponding speckle size. The results of these estimations are shown by the dashed line in Figure 26. The corresponding average far-field speckle size is $195nm$.

Considering that the formation of speckles is governed by Gaussian statistics, the near- and far-field speckle size were experimentally estimated and their values were explained by the homogeneous, planar source model. Intensity and field correlation lengths measured in the far-field, i.e. several wavelengths away from the surface, do not change when increasing the distance from the interface. In the near-field however, we found that the intensity and field correlation lengths have a nontrivial dependence on the distance from the physical interface and, moreover, we have shown that the near field spatial coherence length can have values smaller than the wavelength of radiation. This is explained by the fact that coherence properties of random media at subwavelength scales are determined by both homogeneous and inhomogeneous waves.

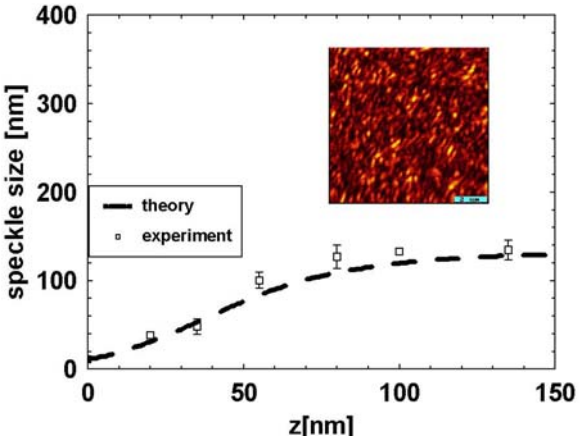

Figure 26: Measured near-field specke size as a function of the distance z from the surface for VYCOR glass sample. The inset shows a typical near-field intensity distribution.

As can be seen, the model of a planar source qualitatively describes second-order statistical properties of the field emitted at the surface of a highly random medium, providing a direct relationship between the statistical properties of the optical near-field and the statistical properties of an equivalent planar source of radiation. However, a relation between the field statistics and the physical properties of the medium would require the description of the field on a surface that has transverse spatial frequencies. For this, a full three-dimensional linear scattering treatment is necessary which is a difficult task when the surface is described only by its statistical properties. In other words, diffraction effects with both homogeneous and inhomogeneous wave contributions need to be included. The situation is complicated even more by the fact that the incident field itself contains both homogeneous and inhomogeneous components making the mapping between the incident and scattered field a tremendous task. In general, the magnitude of an evanescent component depends on all three-dimensional spatial Fourier components of the scattering potential as opposed to one-to-one mapping of between the homogeneous components of the scattered field and the low-frequency components of the scattering potential [52].

3.2 "Far-field" spatial coherence properties - relation to interface statistics

At a few wavelengths away from the physical interface of the random medium, where no evanescent waves are present, a relation between field statistics and the physical properties of the medium might not require a full 3D linear scattering treatment of the field. One could imagine again the predictions of the optical coherence theory corresponding to practically infinite source of radiation [5]. However, we would like to emphasize

that these predictions do not account for detailed surface characteristics. Note also that classical measurements of spatial coherence properties are usually performed at much larger distances z where the limited size of the source cannot be ignored and where the size of the coherence area is actually determined by the extent of the source as mentioned before [53].

On the other hand, the real scattering media have rough interfaces which may affect the field correlation in the neighborhood of the surface. As a result, the statistical characteristics of the interface are expected to also influence the spatial coherence properties of the radiation emitted. In other words, the field coherence properties of the radiation originating from a bounded random medium should relate to the statistical characteristics of its interface.

The angular dependence of light which is diffusely transmitted through or emitted within a random volume-scattering medium (VSM) with absorbing boundaries is well described by the diffusion theory and it is known to have a cosine distribution [6]. However, sometimes real scattering media are bounded by interfaces which manifest refractive index mismatch and, moreover, are rough on the scale of the wavelength. As a result, the boundary conditions for the radiative transfer equation are modified and the angular distribution of the intensity $J(\theta)$ changes. The effect of a real surface can be accounted for by considering an "effective" planar interface that radiates an intensity with an angular distribution different from the classical cosine dependence.

3.2.1 Cross-spectral density dependence on surface statistics

In this section we are concerned just with the homogenous components of the cross spectral density function as there are no evanescent waves contributions at a few wavelengths of light away from the physical interface.

The radiant intensity is directly proportional with the inverse Fourier transform of the cross-spectral density function in the plane of the source [5]

$$J_\omega(\mathbf{s}) = k^2 A\tilde{F}(ks_x, ks_y, \omega)\cos^2\theta, \tag{20}$$

where A is the source area and θ is the angle that the vector $\mathbf{s}$ makes with the normal to the source.

It follows from Equations (18)and (20), after changing from Cartesian coordinates to polar ones, i.e. using $\Delta x = r\cos\varphi$, $\Delta y = r\sin\varphi$ and $s_x = \rho\cos\phi$, $s_y = \rho\sin\phi$, that

$$W(r,\omega) = \frac{1}{A}\int_0^{2\pi}\int_0^1 \frac{J(\arccos(\sqrt{1-\rho^2}))}{1-\rho^2}\exp(ikr\rho\cos(\varphi-\phi))\rho d\rho d\phi. \tag{21}$$

This analysis suggests a way to predict the field coherence length σ_μ when the interface statistics is known. Using Equation (21), the cross spectral density can be numerically estimated for different distributions of the radiant intensity. Moreover, $J(\theta)$ relates to statistical properties at the surface of the sample. In order to obtain the transmitted light distribution as a function of the scattering angle, one has to develop a statistical description of the surface. For the surfaces of interest here, the statistical character of the surface can be simply described by the probability density function of the

random inclination of the surface normal with respect with z axis (local slope). In many cases one can also assume that the distribution of the local slopes is Gaussian with zero mean and has a standard deviation σ_s.

For highly inhomogeneous media, one can consider that unpolarized light is incident upon the interface from the dense medium and that the intensity has a cosine angular distribution. Knowing the probability density for the local slope and using Fresnel's coefficients one finds that the radiant intensity $J(\theta)$ is given by [54]

$$J(\theta) = \int_{-\pi/2}^{-\pi/2} S(\alpha - \arcsin(\frac{n_2}{n_1}\sin(\theta+\alpha)))T(\arcsin(\frac{n_2}{n_1}\sin(\theta+\alpha)))P(\alpha)d\alpha, \qquad (22)$$

where $P(\alpha)$ is the probability density function of the local slope, n_2, n_1 are the refraction indices defining the surface, $S(x) = \cos(x)$ represents the angular distribution of the incident intensity, and $T(x)$ is the depolarized transmittance calculated as the average of the TE and TM transmittances. Because we are interested just in the homogeneous part of the cross spectral density function, the radiation with angles of incidence beyond the critical angle does not contribute to the outgoing intensity.

The simple model taking into consideration the statistical character of the surface and the reflective nature of the boundary can explain the change in the angular dependence of radiant intensity $J(\theta)$. The procedure allows for both local slope standard deviation and the refractive index contrast to be accounted for. In this way, the angular distribution of the emitted intensity is directly related to the statistical properties of the real surface.

In Figure 27, the values of the field coherence length σ_μ, defined as the $1/e$ values of the cross spectral density, are plotted as a function of σ_s, the standard deviation of the

local slope. The calculations presented are for $\lambda = 488nm$ and account just for the homogeneous components of the field. Figure 27 represents the numerical evaluations of the field coherence length σ_μ using the procedure outlined above, when the local slope density probability distribution is considered to be a Gaussian with zero mean and standard deviation σ_s. One can see that σ_μ decreases with local slope standard deviation σ_s. Also, for large values of σ_s, when the radiant intensity $J(\theta)$ tends to a cosine angular distribution, the values of σ_μ decrease towards the coherence length for which $\sin(k\sigma_\mu)/k\sigma_\mu = 1/e$.

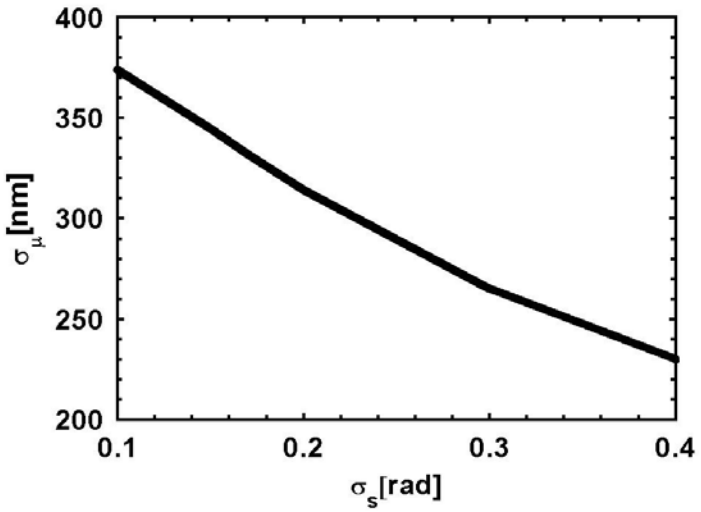

Figure 27: Field coherence length σ_μ as a function of the standard deviation σ_s of local slope. The probability distribution function of the local slopes is a Gaussian function with zero mean and σ_s standard deviation. The calculations are for an index of refraction $n = 1.5$ and light wavelength $\lambda = 488nm$. The field correlation length is estimated from $1/e$ values of the cross spectral density function $W(r, \omega)$.

This result can be easily understood. Rough interfaces have the tendency to diminish the refractive index contrast between the bulk and the outside, and therefore

lead to a Lambertian source behavior corresponding to absorbing boundary conditions. The simple interface model together with the planar source concept explain how the field coherence properties near the source surface (at distances larger that the wavelength of light) depend on the statistical properties at the sample interface.

3.2.2 Spatial coherence dependence on the surface local slope

The theoretical predictions of the dependence between the cross spectral density function and the local slope probability density function have also been examined experimentally. The data were collected on compact slabs made of calcium carbonate and kaolin microparticles with an average diameter of $400nm$ and on slabs containing polystyrene spheres of $356nm$ diameter. Our results refer to physical situations where media with strong volume randomness are bounded by relatively smooth surfaces with slowly varying interfaces. The r.m.s. heights of the surface are typically in the range of $\lambda/4$ to $\lambda/2$. However, the correlation lengths of the scanned surfaces are larger than the wavelength of light, ranging from $3\lambda/2$ to 3λ.

The intensity distributions are measured by scanning across the sample at a constant distance z and collecting images over a 5x5 microns area. We evaluated numerically the field correlation functions and estimated the average radius of the cross section area where the field correlation decreases at $1/e$ of its maximum and consider the width of the field correlation as a measure of the field coherence length. Typical values of the experimental field coherence length $\sigma_{\mu}^{\exp}$ and of local slope standard deviation σ_s are presented in Figure 28.

A direct comparison between the experimental data and the theoretical values of the coherence length σ_μ^{th} is also shown in Figure 28. The theoretical values σ_μ^{th} were calculated using the experimental values of the local slope probability density functions and Equation (21). The local slopes and their standard deviation σ_s were determined from the AFM topographical experimental data and the heights were sampled with a lateral or vertical step which equals the size of the tip. Note that experimental values of the local slope probability density function used in the calculations labeled by triangles in Figure 28 can be different from the Gaussian slope distribution with zero mean assumed in the theoretical results presented as a continuous curve in Figure 28.

A remarkable agreement is obtained with the simple model described here; the discrepancy between the theoretical and experimental values of the coherence length is less than 10%. One can conclude that concept of a planar source together with the model for the angular distribution of the radiant intensity describes qualitatively the second-order statistical properties of the field emitted close to the surface of a highly random medium. It also provides a direct relationship between the measurable statistical properties of the optical field at several wavelengths away from the surface and the statistical properties of an equivalent planar source of radiation which, in turn, are determined by the physical properties of the random medium. At a several wavelengths away, the spatial coherence length of the field does not change anymore as a function of the distance from the interface as in the case of near-field described in the previous section. However, the spatial extend of the field coherence function is influenced by the statistical characteristics of the interface.

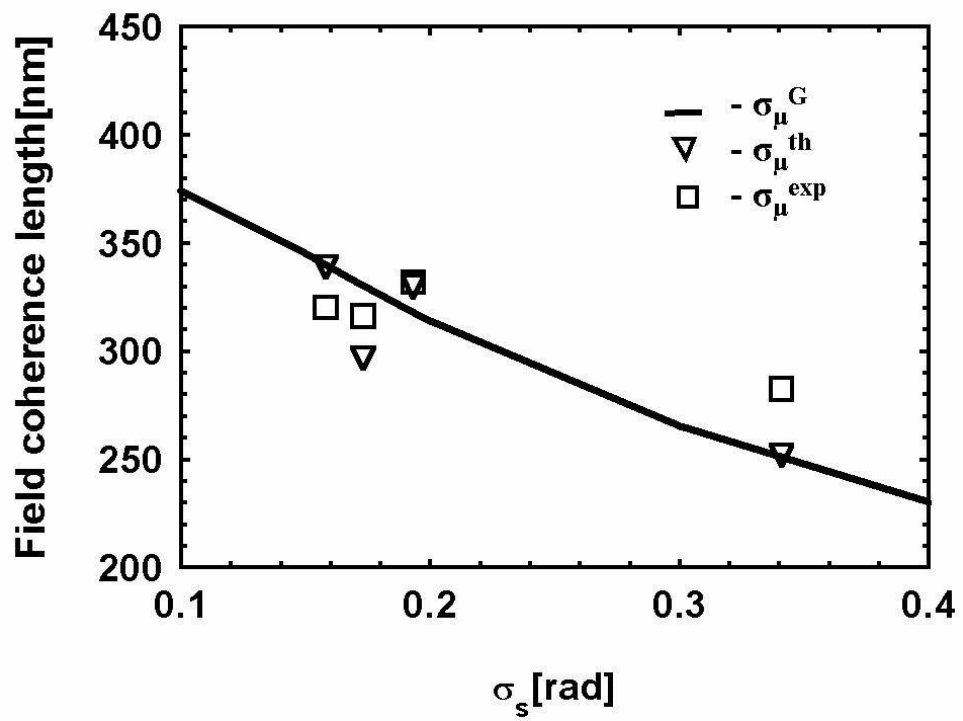

Figure 28: Field correlation length as a function of the standard deviation σ_s of local slope : a) field coherence length σ_μ^G obtained using a Gaussian distribution with zero mean and standard deviation σ_s for the local slope probability distribution function. b) field coherence length σ_μ^{th} obtained using the experimental probability distribution function for the local slopes of the sample examined. c) coherence length $\sigma_\mu^{\exp}$ measured for the same samples. All calculations are for an index of refraction $n = 1.5$ and light wavelength $\lambda = 488nm$.

These results suggest a number of applications. The morphological details at the surface of a random medium affect both the angular distribution of the radiant intensity and the spatial coherence properties of the radiation emitted. Measurements of the angular distribution of far-field intensity require large sample sizes. Because of the natural sizes of the VSM involved in situations of practical interest, far-field measurements may need special optical arrangements or they could simply be impossible. The near-field scanning approach described here can be applied to small-size samples which can still be considered to be a practically infinite source of radiation. Moreover, contrary to a near-field constant distance scanning operation, scanning in constant-height mode at microns away from the surface, permits a non-contact, noninvasive characterization of inhomogeneous interfaces. This NSOM collection mode can be considered as an intrinsically passive optical method for surface characterization which may also be of practical use in some biological applications.

In conclusion, near-field optical techniques have been used to study coherence properties of optical fields close to the interface of a random media. At subwavelength distances, due to the evanescent waves contribution, the extent of the coherence length is z-dependent and also smaller than the wavelength of light. At a few wavelengths away from the interface, where just propagating waves are detected, the spatial coherence properties of the field are z independent and relate to the surface statistics. The small dimensions of both the probe and the scanning area allow one to consider the random medium as a homogeneous, planar, infinitely extended source of optical radiation. This concept provides a good interpretation for the experimental values of the field coherence

length in the vicinity of the surface. Together with a simple interface model, it can also describe the dependence of the "far-field" coherence length on the standard deviation of the local slope.

CHAPTER FOUR: SPECTRA OF LIGHT CLOSE TO INTERFACES

In the previous chapter it was shown that the spatial extent of the field-field correlations in the near-field of a random medium dependents on the distance from the interface and can be even smaller than the wavelength of light. This was explained in terms of an equivalent source whose cross-spectral density function is influenced by the contributions arising from evanescent components of the field. Another physical property of random fields is their spectral density. By definition, as described in Equation (5) the spectral density is a particular case of the cross-spectral density function. Therefore, as the spatial coherence properties at subwavelength scales are influenced by the evanescent waves, one should also expect that the contribution of the evanescent waves would also determine changes in the near-field spectra of light.

It is now generally recognized that the spectrum of light changes even as a result of free-space propagation [55]. However, these studies referred to far-field phenomena and do not account for the contribution of the short-range inhomogeneous components of emitted radiation. Recently, the evanescent components of the field close to the source have also been considered theoretically and differences between near- and far-field spectra of thermal emitted light have been suggested [47, 56].

4.1 Spectral density in the near field of a homogeneous, planar, statistically stationary source of optical radiation

So far we have considered the surface of the random medium as being equivalent to a homogeneous, planar, statistically stationary source of optical radiation. This source, located at $z = 0$, generates, in the half space $z > 0$, a cross-spectral density function which can be decomposed in low- and high-frequency components as shown in Section 1 of Chapter 3. It follows from Equation(13) that the spectral density, defined by Equation(5), can be also calculated anywhere in the half space $z > 0$

$$S(z, \lambda) = S_{\text{hom}}(\lambda) + S_{ev}(z, \lambda), \tag{23}$$

where $S_{\text{hom}}(\lambda)$ is the homogeneous wave contributions to the spectrum, $S_{ev}(z, \lambda)$ is the evanescent one, and λ is the wavelength of light.

The spectrum $S(z, \lambda)$ is practically determined by the spectrum of light in the plane of the source $S^{(0)}(\lambda)$ and by the spectral degree of coherence in the source plane at $z = 0$ [56]. As in the previous chapter, one can consider that the source is characterized by a Gaussian spectral degree of coherence with the field correlation length σ in the plane of the source. We are referring here to situations where the radiation propagates a few wavelengths away from the surface of the source. Therefore, one can consider the source as having a spectrum invariant in propagation [1]. Such sources generate fields whose normalized far-zone spectra are the same as the normalized source spectra. Then, $\sigma = \delta/k$, where δ is a constant and $k = 2\pi/\lambda$. Note that such a source, so called scaling law source, generates in the far zone speckles with sizes that scale with the coherence

parameter δ, while the spectral density $S_{\text{hom}}(\lambda)$ is proportional with the one in the plane of the source $S^{(0)}(\lambda)$. Using $r = 0$ in Equations (18),(19) one can obtain the homogeneous and inhomogeneous parts of the near-field spectral density as

$$S_{\text{hom}}(\lambda) = \pi\delta^2 S^{(0)}(\lambda) \int_0^1 \rho \exp(-\frac{\delta^2\rho^2}{2}) d\rho \tag{24}$$

and

$$S_{ev}(z,\lambda) = \pi\delta^2 S^{(0)}(\lambda) \int_1^\infty \rho \exp(-\frac{\delta^2\rho^2}{2}) \exp(-2kz\sqrt{\rho^2-1}) d\rho, \tag{25}$$

Using the results in Equations (23),(24),(25), we calculate the spectral density for different distances z and for different values of the field correlation length at $z = 0$. To illustrate the effect of high-frequency components on the spectrum, we consider a Gaussian spectral density in the plane of the source, $S^{(0)}(\lambda) = \exp[-(\lambda-\lambda_0)^2/\Delta^2]$, with $\lambda_0 = 600nm$ and $\Delta = 80nm$. All spectra are normalized by their respective maxima. Figure 29 presents $S_{ev}(z,\lambda)$ at $z = 100nm$ and $z = 300nm$ from the plane of the source. The calculations were carried out by accounting for both homogeneous and inhomogeneous contributions; the corresponding spectrum $S(z,\lambda)$ at a distance $z = 100nm$, is also shown in Figure 29. At $300nm$ away from the source interface, due to the weak evanescent contribution, the total spectral density is practically given just by its low-frequency components, i.e. the total spectrum $S(z,\lambda)$ at $z = 300nm$ coincides with the far-field one, almost overlapping with $S^{(0)}(\lambda)$. The inset in Figure 29 presents the ratio between the deviation of the evanescent spectral density with respect to the spectral density in plane of the source and the width of $S^{(0)}(\lambda)$, as a function of δ. The wavelength shift and the Gaussian width are estimated where the spectrum decays at $1/e$ of its maximum. The calculations are for

$\delta = 3\pi/10$ and for a distance $z = 100nm$ away from the surface of the source. One can see that the evanescent waves tend to shift the spectrum of light toward larger wavelengths and that this spectral shift decreases with the coherence parameter δ in plane of the source.

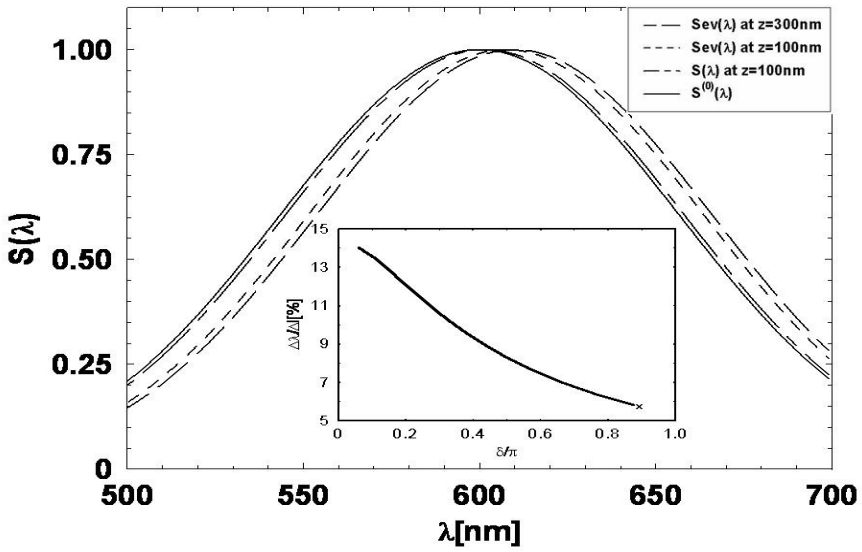

Figure 29: Normalized spectral density for $z = 100nm$ and $z = 300nm$ away from the surface. The calculations are for $\delta = 3\pi/10$ and account for both homogeneous and inhomogeneous contributions. The inset presents the ratio between the deviation of normalized $S_{ev}(z, \lambda)$ from the $S^{(0)}(\lambda)$ and the width of $S^{(0)}(\lambda)$, as a function of the coherence parameter δ in plane of the source, for $z = 100nm$ and $S^{(0)}(\lambda) = \exp[-(\lambda - \lambda_0)^2/\Delta^2]$, with $\lambda_0 = 600nm$ and $\Delta = 80nm$.

4.2 Experimental results

We measured the spectrum of light near the surface of various random, highly scattering media which were illuminated in a transmission geometry. A white LED is

used to illuminate the random medium and the transmitted field is coupled to the cantilevered near-field optical force sensor with a $500nm$ aperture, while the scattered light is detected by a spectrum-analyzer. Measurements were performed at the same height z from the sample surface but at different locations on the sample interface. Typically, ten measurements are averaged to build each near- or far-field spectrum.

The data were collected on two different media: compact slabs made of calcium carbonate and kaolin microparticles with an average diameter of $400nm$ and VYCOR porous glass samples with 28% void volume and $4nm$ average pore size. Their scattering properties are characterized by the correlation length of the refractive index fluctuation and by the r.m.s. height of the surface which typically range between 100 and $250nm$ for the microparticles slabs and between 13 and $50nm$ for the VYCOR glass. The r.m.s. heights of the samples are determined by scanning in constant distance mode with a $150nm$ tip aperture. Typical topographical images of the random media described here and their corresponding roughness are presented in Figures 30.

The homogeneous part of the spectral density, $S_{\text{hom}}(\lambda)$, is measured at distances ranging between 1 and $2.5\mu m$ away from the physical interface of the sample. In all cases, we recover the same spectra, irrespective of the distance z from the interface. The total spectrum of light, $S(z, \lambda)$, is measured in the near-field of the sample where both homogeneous and inhomogeneous waves contribute and, using Equation(23), the evanescent part of the spectra is estimated. The experimental noise is subtracted and all spectra are normalized by their maxima. The near-field spectral densities are measured at $z = 200nm$ in the case of the calcium carbonate slabs and at $z = 130nm$ for the

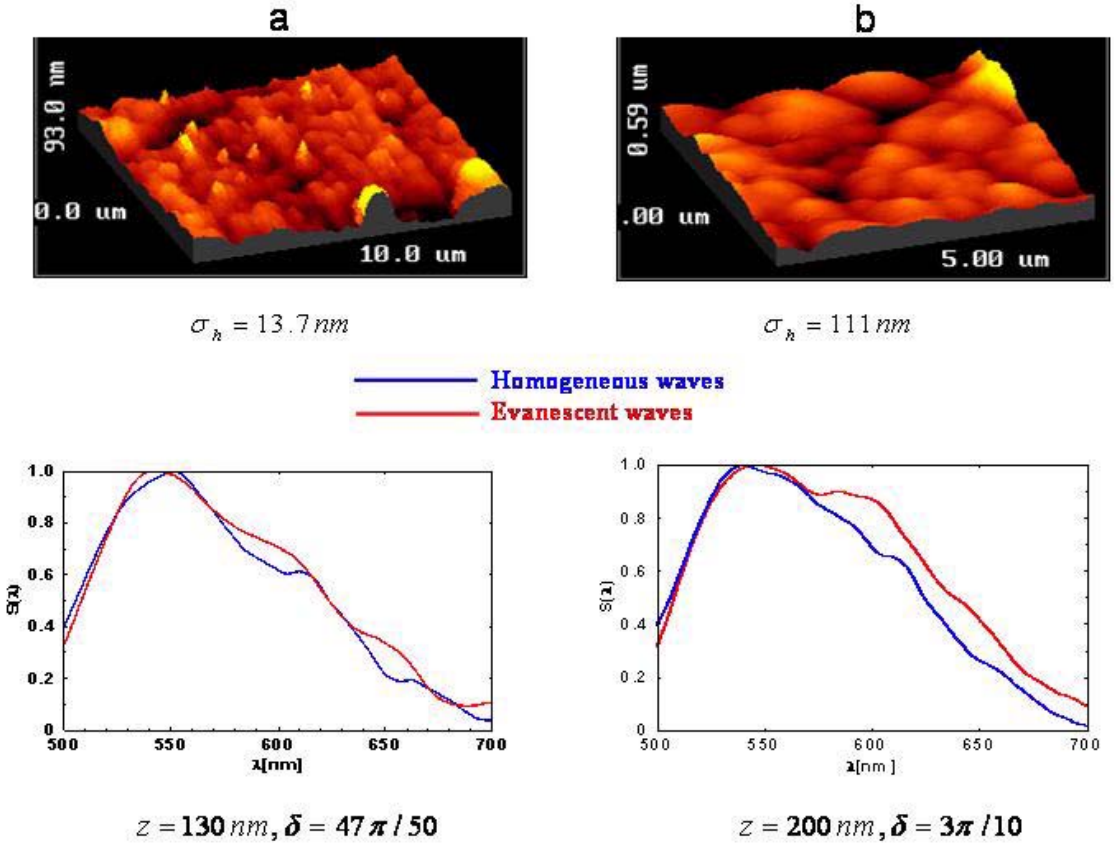

Figure 30: a)Topography and spectra of light of a VYCOR glass sample; the r.m.s roughness is $13.4nm$ and $\delta = 47\pi/50$ (b) Topography and the spectra of light of a compact slab made of calcium carbonate and kaolin microparticles with an average diameter of $400nm$; the r.m.s roughness is $111nm$ and $\delta = 3\pi/10$.

VYCOR glass. The experimental data obtained for calcium carbonate slabs are presented in Figure 31. They are also compared with the theoretical predictions of Equations(23), (25), and the results are shown in the same figure. For the case where the correlation length σ in plane of the source is inverse proportional with the wave number, $\sigma = \delta/k$, for δ being constant, the homogeneous, planar, statistically stationary source concept of optical radiation gives a normalized far-field spectrum identical with the one in plane of the source. This allows us to consider the experimental far-field spectrum of light as $S^{(0)}(\lambda)$ and to theoretically estimate, using Equations (23)-(25), the total near-field spectral density $S(z, \lambda)$ and its evanescent part $S_{ev}(z, \lambda)$.

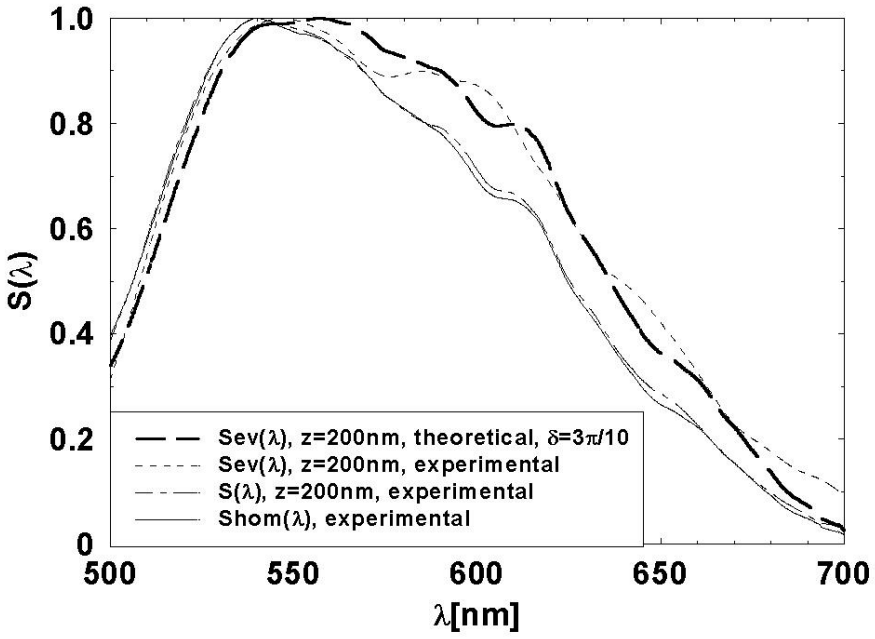

Figure 31: Measured far-($z = 1500nm$) and near-field ($z = 200nm$) normalized spectra corresponding to the compact slab made of calcium carbonate and kaolin microparticles. Also shown is the prediction of Eq. (23) for the case of $\delta = 3\pi/10$.

The comparison between the experimental and theoretical spectra permits estimating the field coherence in plane of the source given by δ, which, in turn, is determined by the physical properties of the random medium. As illustrated in Figures 30, a value of $\delta = 3\pi/10$ was obtained for the slabs made of microparticles with an average diameter of $400nm$, while for the VYCOR glass, we estimated $\delta = 47\pi/50$. For each sample, the same value of δ was obtained by fitting both the total near-field spectrum and just its evanescent part.

In general, the coherence properties in plane of the random media are characterized by the correlation length of the refractive index fluctuations and by the r.m.s. height of the surface topography. Large field correlation lengths of the equivalent planar source of radiation source correspond to a small roughness of the physical interface, as can be seen in Figures 30. The homogeneous, planar, statistically stationary source model described above also predicts a far-field coherence length which is proportional with δ and therefore, is inversely proportional with the surface roughness. This is in full agreement with measurements of the spatial field correlation near random media interfaces describes in Section 3 of Chapter 3. These results also demonstrate that the far-field coherence length decreases when the r.m.s height of the surface of the sample increases.

In this chapter we have shown that based on the same technique of scanning near-field optical microscopy, subtle differences between near- and far-field spectrum of light can be measured and quantified. We found that the red shift of the near-field spectra is controlled by the distance from the interface as well as by the coherence in the plane of the source. We would like to point out that near-field spectral measurements in the proximity

of a random medium have an appealing feature: no scanning is required in order to retrieve information about the coherence properties of the equivalent planar source which relates to the statistics of the real physical interface. Of course, the same information can be extracted from the near-field spatial correlation measurements as shown in Chapter 3. However, in this case, scanning the surface of the scattering medium with a probe with an appropriate aperture is necessary in order to experimentally estimate the near-field spectral degree of coherence.

So far, we have seen that the surface of the random media can be described as a homogeneous, planar, source of optical radiation and that the same interpretation explains different features of the statistical properties of the fields close to a highly inhomogeneous medium. Both the spatial coherence characteristics and the spectrum of light in the vicinity of a random medium depend on the coherence properties of the equivalent source of radiation, which in turn, relate to the surface statistics. Therefore, physical characteristics of inhomogeneous media can be determined by examining various features of the emitted field. For instance, as illustrated in this section, the modifications of the near-field spectra depend on the surface roughness. Alternatively, as we have shown in Section 3 of Chapter 3, the local slope standard deviation of the local surface slope can be retrieved from the spatial extend of the far-field correlation lengths.

CHAPTER FIVE: NON-GAUSSIAN STATISTICS OF LIGHT FLUCTUATION IN THE NEAR-FIELD OF RANDOM MEDIA

When a random interference pattern is produced by overlapping sinusoidal waves having random phases, the process can be modeled as a typical two-dimensional random walk problem [2]. It is worth mentioning that the concept of random walk has described successfully a number of optical phenomena obeying both Gaussian and non-Gaussian statistics [2],[57],[58]. In the case of quasimonochromatic radiation, the intensity probability density function is evaluated by considering the stochastic process to be a random walk in the complex plane. The approach has been used to describe the formation of the far-field speckles but it can also be applied in the near-field, where the evanescent field components contribute to the statistical properties of the intensity distribution. Depending upon the type of excitation which is produced in specific experimental configurations, different manifestations of the properties of optical fields in the Gaussian and non-Gaussian regimes can be obtained in the near-field of a random, inhomogeneous medium.

In previous chapters we discussed in detail situations which resulted from a global excitation of a random medium. As a consequence, the intensity variations in the near-field of highly inhomogeneous media satisfied the requirements of circular Gaussian sta-

tistics. In this case, the intensity probability density function had a negative exponential dependence and the optical contrast was unity. In the experiments described before, the intensity distributions were collected using a NSOM microscope in transmission-collection mode of operation. In this case when light is transmitted through or is emitted within a highly scattering medium, the first-order statistics of intensity can not be used to infer information about the surface. However, we proved that in this case the second-order statistical properties of the optical near-field depend on the statistical properties of an equivalent planar source of radiation which, in turn, should be determined by the physical properties of the random medium. Now, if it would be to relate the equivalent source model to the physical properties of the random medium, one should bear in mind that the model assumed a planar source and, therefore, the same spectral degree of coherence in the source plane at $z = 0$ for both homogeneous and inhomogeneous contributions. Real scattering media have rough interfaces which may, however, induce different surface coherence effects for low- and high-frequency components of the cross spectral density function. A more refined model would require a full three-dimensional treatment of the field in the neighborhood of the interface.

A different approach can be envisioned in order to use the statistical properties of the fields not only to determine the characteristics of radiation emanating from random systems but also to study various properties of random media. In some practical applications of local excitation of a random medium, the near-field random interference pattern in the neighborhood of the interface may be governed by non-Gaussian statistics.

In this case, the optical contrast is significantly smaller than unity and is dependent on the physical properties of the interface.

When there is a certain correlation between the superposing waves which form a speckle pattern, the statistics of resultant field distribution has a non-Gaussian behavior. A similar situation occurs when the total field is the result of the superposition of a reduced number of independent contributions. This regime is generated when, at a given observation point, the field is not a superposition of a large number of contributions originating from different locations within the random medium. Non-Gaussian statistics may also be the result of weak scattering, when the phases of the elementary scattering centers are not uniformly distributed anymore and their probability density function depends on the surface statistics.

5.1 Experimental situations

Optical fields obeying non-Gaussian statistics are a result of a reduced number of independent contribution and a nonuniform distribution of the phase of elementary scattering centers. The situation is encountered, for instance, when a random medium is locally illuminated by the tip of an NSOM as illustrated in Figure 32. In such illumination-reflection configuration, light is coupled to one end of the fiber and the radiation emanates from the other end which is tapered down to diameter of $100nm$. In the configuration of Figure 32, the radiation is coupled onto the medium which contains subwavelength variations in both the topography and its optical properties, and is then re-emitted in the form of scattered field. During the scattering process, some of the evanescent components are being converted into homogeneous waves, which are then detected in the far field by

an avalanche photodiode. As in the previous case, the NSOM probe has the possibility to scan in constant distance mode and to simultaneously obtain the AFM topography and the near-field optical images.

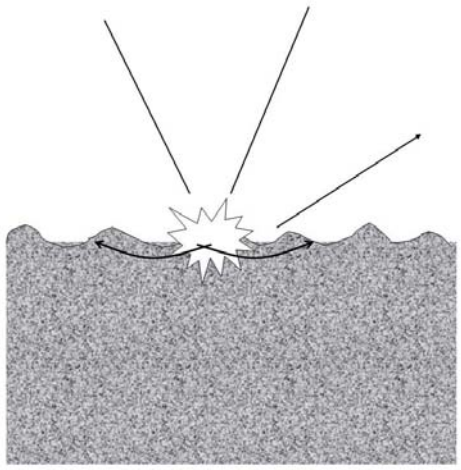

Figure 32: Illumination-reflection configuration of NSOM.

A typical topographical image and its corresponding near-field intensity distribution is presented in Figures 33. The data obtained in the illumination-reflection configuration illustrated in Figure 32 are collected on slabs of calcium carbonate and kaolin microparticles with r.m.s roughness ranging between $\lambda/40$ and $\lambda/10$.

5.2 Probability density function of intensity fluctuations

It is expected that the evanescent waves in the neighborhood of the physical interface of a random medium will carry information about structural details smaller than the wavelength of light. The study of the first-order statistics of intensity fluctuations in the near-field of random media using an NSOM in illumination-reflection configuration can reveal these characteristics.

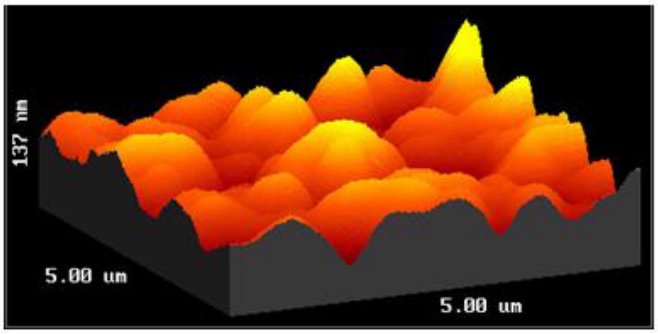

a

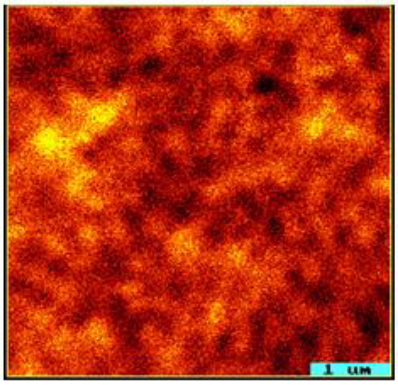

b

Figure 33: (a) Topography of compact slabs made of calcium carbonate and kaolin microparticles; the r.m.s roughness is 22.7nm. (b) Near-field intensity distribution collected over the same area.

When examining the near-field intensity distributions, an interesting observation can be made. The intensity probability density function depends on the measured average intensity, which can be adjusted by changing the incident intensity coupled into the fiber tip. Such a dependence of the statistical properties of the scattered field on the excitation level could not be observed in any of the transmission measurements. The change of the statistics of intensity, i.e. the narrowing of the probability density function when the incident intensity increases, is somewhat puzzling because one should not expect any nonlinear phenomena in the media examined. This behavior observed in the illumination-reflection configuration can be explained by realizing that: (i) the radiation couples onto the medium away from the tip before being re-emitted and (ii) the noise level of the light detection process imposes an inherent intensity cut-off. As a result, as presented in Figure 34, when the incident intensity increases, $I_2^0 > I_1^0$, the detection system collects the radiation $I_2 > I_1$ from a larger area, $A_2 > A_1$, on the surface of the medium. Figure 34 also illustrates the coupling of the radiation into the medium.

Figure 35 presents the measured intensity probability density function $p(I)$ multiplied by the average intensity $\langle I \rangle$, plotted in a logaritmic scale as a function of the normalized point intensity $I/\langle I \rangle$. The data were collected scanning the same area of the sample, the average intensity being the only variable parameter. The change in the average intensity $\langle I \rangle$ is obtained by adjusting the incident intensity. One can notice that, as opposed to the previous case of global excitation of the random media which was discussed in Section 2.3 (see Figure 20), the measured intensities do not obey a negative exponential anymore. Moreover, their intensity probability density function depends on

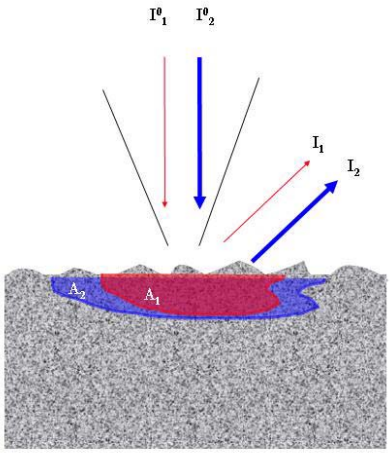

Figure 34: The coupling of the incident intensity $I_2^0 > I_1^0$onto the media and its re-emision $I_2 > I_1$. The detection system collects the re-emitted radiation from an area $A_2 > A_1$ according with the value of the incident intensity.

the average measured intensity $\langle I \rangle$. The corresponding intensity probability density resembles a gamma function while the contrast takes in this case values significantly smaller than unity.

Another important experimental observation is worth noting. The intensity probability density function depends not only on the measured average intensity but also on the surface roughness. This statement is illustrated in Figure 36, where the measured intensity probability density function $p(I)$ multiplied by the average intensity $\langle I \rangle$, is plotted in a logaritmic scale as a function of the normalized point intensity $I/\langle I \rangle$ for an average intensity $\langle I \rangle = 600$kcps. One can notice that the behavior of $p(I)$ changes even for surfaces with slightly different values of the r.m.s. height fluctuations. A small increase in the roughness leads to broadening of the intensity distribution.

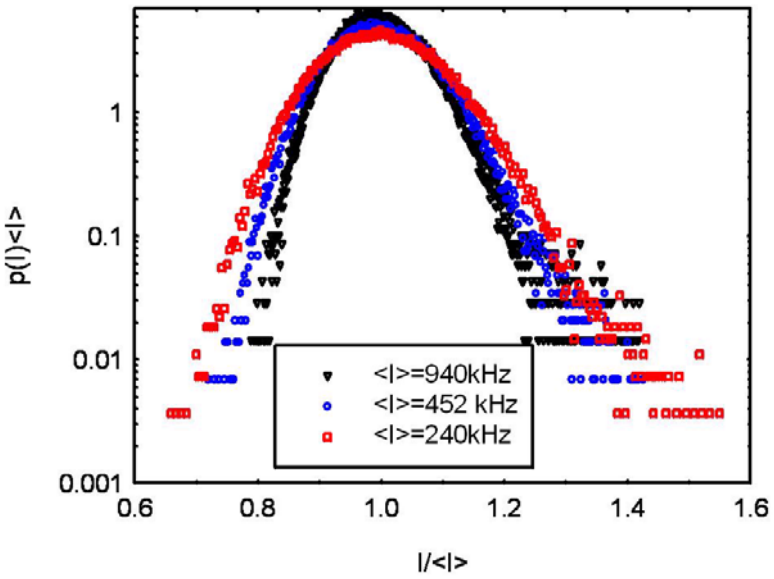

Figure 35: Normalized intensity probability density function measured for different average intensities as indicated.

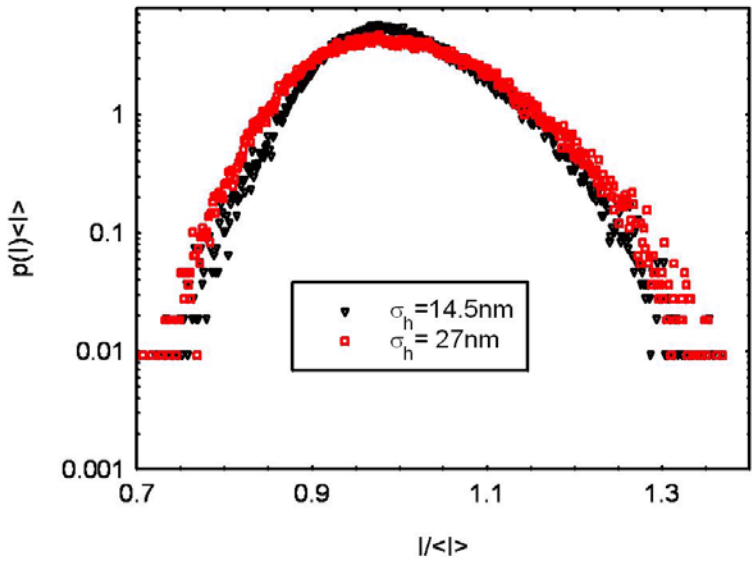

Figure 36: Normalized intensity probability density function measured for different r.m.s height fluctuations of the surface as indicated.

5.3 Optical contrast

A useful concept for characterizing the random interference pattern is the ratio between standard deviation of the intensity fluctuations and the average intensity, the so-called speckle contrast: $C = \sqrt{\langle I^2 \rangle - \langle I \rangle^2} / \langle I \rangle$. We will show that, for some specific cases, the optical contrast of the near-field speckle pattern relates to the statistical properties of the physical interface.

5.3.1 Random walk concept

The interaction between optical waves and random media has been systematically investigated and it is now well understood that the familiar appearance of the speckle patterns can be described in therms of Gaussian and non-Gaussian statistics of light fluctuations. The coherent superposition of the waves generates a speckle pattern whose intensity statistics depend on their number N and on their phase distributions [59]-[61]. The statistics of the random waves interference have been studied in details and it has been shown that, for a given phase distribution, the optical contrast can actually decrease when the number of independent contribution increases [60]. This model considers the interference of waves having equal amplitudes. Their phases are statistically independent random variables, each having a probability distribution of the form:

$$\begin{aligned} f(\theta, \nu) &= (2\pi I_0(\nu))^{-1} \exp(\nu \cos(\theta)),\ \text{-}\pi < \theta < \pi \\ &= 0,\ \text{elsewhere} \end{aligned} \tag{26}$$

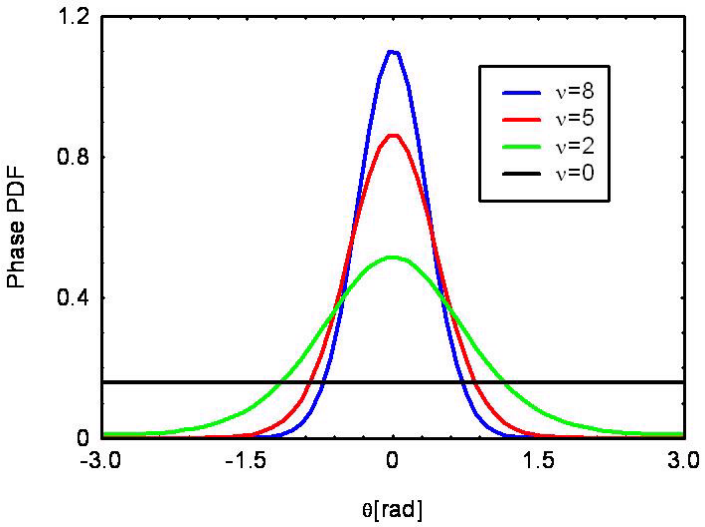

Figure 37: The phase probability distribution function for different values of ν parameter, as indicatted.

where ν is a real nonnegative constant and $I_n(\nu)$ is the modified Bessel function of order n. As illustrated in Figure 37, when $\nu = 0$ this expression reduces to the familiar uniform phase distribution encountered in the speckle patterns obeying the Gaussian statistics. As ν is increases, $f(\theta, \nu)$ becomes bell shaped around $\theta = 0$, reaching for large values of ν the form

$$f(\theta, \nu) = (2\pi\nu^{-1}))^{-1/2} \exp(-\theta^2/2\nu^{-1}). \tag{27}$$

Thus the phase θ is approximately Gaussian distributed with the variance $\Delta\theta^2 = \nu^{-1}$.

The intensity probability density function and the speckle contrast can be evaluated analytically for different phase distributions $f(\theta, \nu)$ and different number of elementary

scattering centers N [60]:

$$C(N,\nu) = \frac{\sqrt{N(N-1)\{1+g_2(\nu)^2-2g_1(\nu)^4+2(N-2)[(1+g_2(\nu)g_1(\nu)^2-2g_1(\nu)^4)]\}}}{N[1+(N-1)g_1(\nu)^2]} \tag{28}$$

where $g_1(\nu) = I_1(\nu)/I_0(\nu)$ and $g_2(\nu) = I_2(\nu)/I_0(\nu)$. We present in Figure 38 this dependence of the speckle contrast on the number N of scattering centers for different values of ν. Interestingly, one can notice that, for a narrow phase distribution, the optical contrast may decrease with N, taking values much smaller than the unity. Moreover, for a given value of N, the random walk model predicts an increase of the optical contrast as the phase distribution broadens. This situation happens, for instance, along the dotted vertical line in the Figure 38.

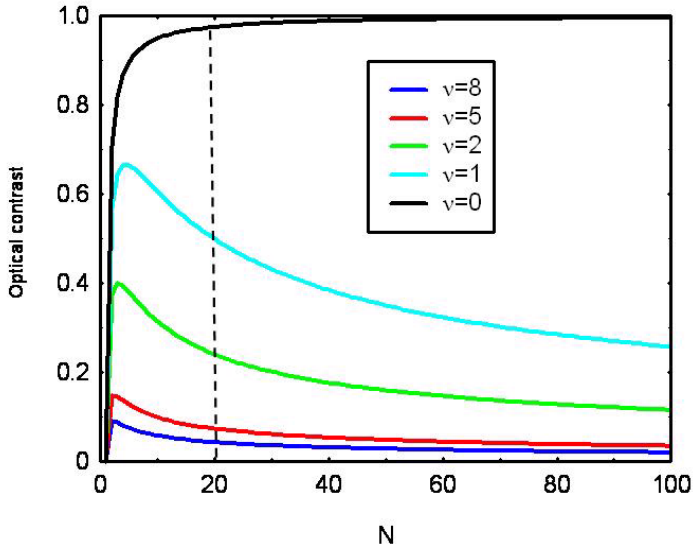

Figure 38: Optical contrast dependence on the number of the scattering centers N for different values of ν parameter, as indicatted. An increase of ν corresponds to narrowing the phase distribution as illustrated in Fig. 37.

Note that the random phasor model also explains the case when the phases of the elementary scattering centers are uniformly distributed ($\nu = 0$). In this situation, also illustrated in Figure 38, the optical contrast increases with N and reaches very fast the saturation value of unity which is characteristic to the Gaussian statistics regime. It is important to realize that it is not only the number of the scattering centers that governs the non-Gaussian regime of the random interference but also the departure of the phase from being uniformly distributed.

5.3.2 Physical situation

For all practical purposes, a simple model can be developed by considering that, due to inhomogeneities in the optical properties, light is first coupled inside the medium over a surface of area A, the size of which depends on the incident intensity as shown in Figure 34. Within this area, N independent elementary scattering centers are being excited which then determine the radiation emitted from the surface. In a first approximation, one can consider that A is proportional with the incident intensity, and so is N.

We can regard these elementary scattering centers as being distributed on the physical interface of the random medium. The radiation couples inside the medium and excites surface and subsurface scattering centers in the corresponding volume $V = A \cdot d$, where d is the penetration depth. The effect of the volume scattering is equivalent with N surface scattering centers distributed on the physical interface of the random medium which have their initial phases θ_i randomly distributed. In steady state, due to the coupling of radiation onto the medium, these elementary scattering centers are not excited

in phase and the distribution of their initial phase θ_i is determined by the local properties of the medium. For simplicity, one can consider the probability density of the initial phase of these elementary scattering centers to be a Gaussian $\frac{1}{\sqrt{2\pi}\Delta\theta_i}\exp(-\frac{\theta_i^2}{2\Delta\theta_i^2})$ with the r.m.s fluctuations $\Delta\theta_i$ depending on the local characteristics of the inhomogeneous medium.

The radiation re-emitted by the N elementary scattering centers is then collected in the far-field, after accumulating an additional phase θ_p, which depends on the distribution of the surface heights. When the excited regions are larger than the lateral correlation area of the surface, the surface statistics is stationary over areas of size A. As the heights of the interface are Gaussian distributed, so will be the additional phases θ_p of the emitted field. The r.m.s fluctuations of this phase are determined by the surface roughness, so that $\Delta\theta_p = k_o\sigma_h$, where k_o is wave number in air and σ_h represents the the r.m.s height of the surface fluctuations. If the phases θ_i and θ_p are statistically independent random variables, the distribution of the total phase of the elementary scattering centers, $\theta = \theta_i + \theta_p$, is also a Gaussian function with the r.m.s fluctuations being $\Delta\theta = \sqrt{\Delta\theta_i^2 + \Delta\theta_p^2}$. The experimental phase distribution is narrow enough to be considered a Gaussian function with the width given by $\Delta\theta = \nu^{-2}$, as discussed in the previous section.

The situation can be now regarded as a practical case of a coherent superposition of waves scattered by N independent but identical elementary scattering centers and can be described as a random walk in the complex space. The amplitudes and the phases of the field emitted by the elementary scattering centers are statistically independent random variables. Moreover, as the elementary scattering centers reemit radiation after reaching the steady state, the amplitudes of the emitted field can be considered to be all equal

deterministic constants. However, as opposed to the transmission-collection configuration discussed in Chapter 3, the phases of the scattered field are not uniformly distributed anymore. Their probability density function is approximated by a Gaussian distribution with the r.m.s phase fluctuations $\Delta\theta$ determined by both surface ($\Delta\theta_p$) and subsurface ($\Delta\theta_i$) properties of the inhomogeneous medium.

5.3.3 Experimental results

The simple model outlined above provides a good description of the experimental results. Typical values of the measured optical contrast are shown in Figure 39 for different surface roughness and for different average intensities, which were adjusted by modifying the excitation level. The data were recorded over areas of 5x5 microns situated at the same distance z from the surface. In order to explain the experimental data, let us consider that the average intensity $< I >$ over the scanning area is proportional with the incident intensity or, in other words, with the number of elementary scattering centers $< I >= \alpha N$. Note that even if the number N of the elementary scattering centers increases when the excitation level increases, their phase distribution does not necessarily change. This is a consequence of the fact that the effective local properties of the medium are the same irrespective of the size of the illuminated area.

In Figure 39, each curve is evaluated using Equation (28) for a certain value of the coupling parameter α and for a Gaussian phase distribution with the width $\nu^{-2} = \Delta\theta = \sqrt{\Delta\theta_i^2 + \Delta\theta_p^2}$. In this evaluation we used: (i) $\Delta\theta_p = k_o\sigma_h$ with σ_h being the measured AFM roughness of the scanned area and (ii) $\Delta\theta_i = 0.268$rad, which was found to best fit

all the experimental data collected on surfaces with different r.m.s. height fluctuations. This value of $\Delta\theta_i$ should relate to the local fluctuations of the dielectric constant and it is therefore material dependent. The relation between the initial phase distribution of the elementary scattering centers and the local characteristics of the inhomogeneous medium can be established based on a microscopic model of the local dielectric function. For the purpose of our discussion, however, it is important to realize that the constant value of $\Delta\theta_i$ reflects the fact that the local optical properties are independent not only of the size of the illuminated area but also of the surface roughness. As pointed out before, the simple model of the coherent superposition of waves allows for both surface ($\Delta\theta_p$) and subsurface ($\Delta\theta_i$) effects to be accounted for.

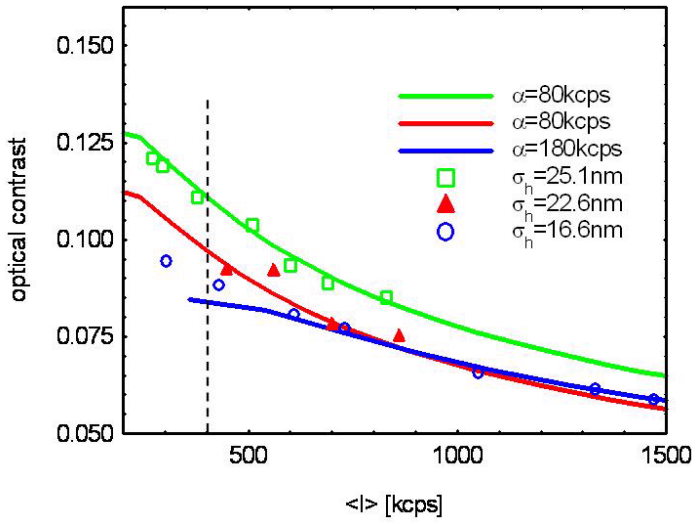

Figure 39: The dependence of the optical contrast on the average intensity for different r.m.s roughness of the surface as indicated. The symbols represent typical experimental data and the curves are the theoretical predictions based on the random walk model of Ref. [60] for $\Delta\theta_i = 0.268$rad.

The number N of elementary scattering centers can now be inferred using the fitting procedure illustrated in Figure 39. For a better illustration, we present in Figure 40, using Equation (28), the theoretical estimation of the contrast as a function of the number of the elementary scattering centers N. The figure also points out the experimental values of the optical contrast and of the corresponding N for an average intensity of 400kcps (the vertical dotted line in Figure 39) and for different roughness. One can notice that, for a certain value of N, the random walk model predicts an increase of the optical contrast with the roughness of the interface (the dotted vertical line in the inset of Figure 40). Practically, as illustrated by the symbols in Figure 40, one should expect that the rougher the scanned surface, the larger the number of individual contributions to the measured intensity.

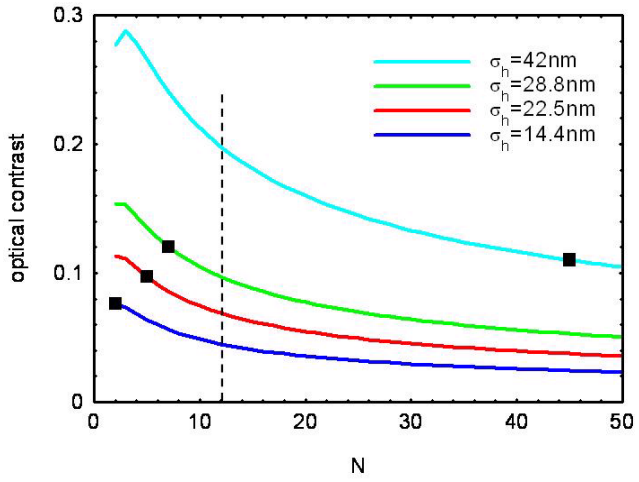

Figure 40: Optical contrast as a function of the number N of elementary scattering centers for different values of the surface roughness. The points are the experimental values of the contrast and the corresponding values of N for an average intensity of 400kcps as indicated by the vertical dotted line in Fig. 39.

An important conclusion follow from the data analysis presented above. The statistical properties of the optical radiation relate to the statistical properties of surface. The dependence of the optical contrast on the surface roughness is shown in Figure 41 where the experimental results correspond to an average intensity of 400kcps. The curves are the predictions of the random walk model evaluated for $\Delta\theta_i = 0.268$rad, $\Delta\theta_p = k_o\sigma_h$ and for the number of elementary scattering centers N estimated from the fitting procedure illustrated in Figure 39. We remark that, for relatively smooth surfaces, the non-Gaussian near-fields have an optical contrast which increases with the r.m.s roughness of the physical interface. It is also interesting to note that, when the surface becomes rougher, more independent scattering centers tend to contribute to the detected intensity. However, the intensity distribution is still non-Gaussian because the phases of the elementary scattering centers are not uniformly distributed.

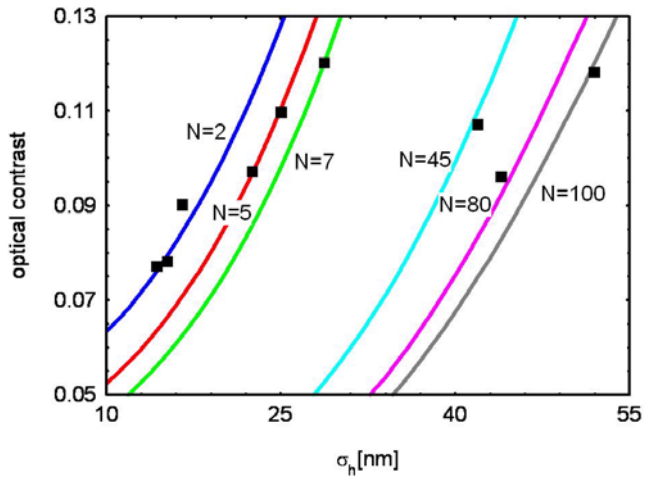

Figure 41: The dependence of the optical contrast on the surface roughness. The symbols denote the experimental data measured for an average intensity $< I >= 400$kcps while the curves represent the predictions of the theoretical model for $\Delta\theta_i = 0.268$rad.

In conclusion, we have shown that, when randomly inhomogeneous media are excited locally, in an illumination-reflection geometry for example, the near-field speckle patterns are governed by non-Gaussian statistics and, consequently, the optical contrast is significantly smaller than unity. We have shown that, in practice, the probability density of the scattered intensity depends on the physical properties of the interface and also on the incident light intensity. We have demonstrated that, in this situation, the stochastic properties of the scattered intensity can be used to determine the statistical properties of the physical surface.

When the experimental configuration is properly accounted for, a simple model considering the superposition of waves having random phases can describe both statistical regimes encountered in the near-field of random media.

The situations discussed in this chapter illustrate another aspect of the coherence properties of optical radiation in the proximity of random media. We have shown that different statistical properties of optical near-fields result from different exitation-detection configurations. The results included here are useful not only for understanding the radiation coupling in and out from inhomogeneous media but they could also lead to different methodologies for characterizing surface and subsurface phenomena.

CHAPTER SIX: SUMMARY OF ORIGINAL CONTRIBUTIONS AND CONCLUSIONS

Near-field optics is most of the time discussed in the context of near-field microscopy. The primary motivation for the development of this field is the use of electromagnetic fields to obtain imaging superresolution. Recently, an entire class of novel technologies has emerged which relies on nonpropagating fields for exciting or detecting radiation at subwavelength scales.

In this thesis, concepts specific to near-field optics and experimental capabilities specific to near-field microscopy were used to investigate the various aspects of coherence properties of random electromagnetic fields in vicinity of highly inhomogeneous media.

Optically inhomogeneous media which emit or scatter radiation are typical examples of real systems that can generate random electromagnetic fields. The properties of these fields can be characterized only within the frame of the coherence theory. The specific features of random fields at subwavelength distances from the surface of the real media are influenced by the presence of evanescent waves because, in this case, both propagating and nonpropagating components contribute to the detectable properties of the field. In

our studies, we have fully accounted for both contributions and, as a result, different surface and subsurface characteristics of the inhomogeneous media could be explained.

Cutting-edge technology in the near-field optical microscopy offers the possibility to construct optical images with resolution of about $\lambda/10$ while detecting extremely low light levels, often in photon-counting mode. In particular, we have shown that, the sub-wavelength resolution of the near-field scanning optical microscope and its capability to acquire simultaneously 3D topography and optical intensity images permits studying the properties of the random optical fields near the surface of real media accounting therefore for both propagating and evanescent waves and also for subtle surface and subsurface effects[1].

As a result of specific experimental configurations for exciting the highly inhomogeneous media, different regimes are obtained for the statistics of the emitted field. We have demonstrated that fluctuating optical fields in the neighborhood of a random medium can exhibit either Gaussian or non-Gaussian statistics.

A situation of global excitation is established in a transmission-collection geometry where the intensity variations in the near-field of a highly inhomogeneous medium satisfy the requirements of circular Gaussian statistics[2]. In this case, the multiple scattering in the bulk completely randomizes the directions and the phases of the waves reaching the surface and a large number of independent scattering centers contribute to the field in each detection point. As a result, the intensity probability density function has a negative

[1] A. Apostol, J. Biggerstaff, A. Dogariu, K. Olvey, "Near field fluorescence imaging of A375 Human Melanoma Cells", OSA Technical Digest, 427, (2002).

[2] A. Apostol, A. Dogariu, "First and second-order statistics of optical near fields", Optics Letters, 29, 235 (2004).

exponential dependence and the intensity contrast is always close to unity. This happens at subwavelength scales, in the near-field of random media and also in the "far-field", i.e. at several wavelengths away from the surface, and permits examining the second order statistical properties of optical fields in the vicinity of interfaces.

The propagation vectors of the waves at the interface together with the topographical characteristics of the surface determine both propagating and evanescent waves in the near-field of the medium. In the close vicinity of the surface, the optical probe collects both the homogeneous and inhomogeneous components of the emitted field. The influence of evanescent fields was experimentally demonstrated by the exponential decay of the measured intensity with the distance z from the physical interface[2]. As expected, this contribution vanishes at distances z larger than the wavelength of light, where only the homogeneous components are contributing.

A description of the near-field distribution can be developed if the surface of the random medium is considered to be equivalent to a homogeneous, planar, statistically stationary source of optical radiation. Due to the small dimensions of both the scanning area and the probe, the surface of the sample can be considered to be an infinitely extended source of optical radiation. When propagating and evanescent waves contributions are fully accounted for, the homogeneous planar source model explains both the spectrum of light[3] and the spatial coherence properties in the vicinity of the interface[4].

[3] A. Apostol, A. Dogariu, "Light spectra in the near-field of random media", Optics Letters, 29, 920 (2004).

[4] A. Apostol, A. Dogariu, "Spatial correlations in the near field of random media", Physical Review Letters, 91, 093901 (2003).

One aspect of random optical fields is their spectral density. We experimentally demonstrated for the first time that differences between near- and "far-field" spectra of radiation are determined by the high-frequency components of the spectral density that are associated with the evanescent field near the surface and, therefore, are z-dependent[3]. Our results show that the state of coherence in the plane of the source affects the near-field spectral shift toward larger wavelengths (red shift). On the other hand, the coherence properties in the plane of an equivalent source situated at the surface of the medium are determined by the r.m.s. height fluctuations of the interface and, therefore, the near-field spectrum of light scattered by random media can provide direct information about the statistical properties of the interface.

Another characteristic of random optical fields is the extent of their spatial correlations. We demonstrated that, at subwavelength scales, where the coherence properties of optical fields are influenced by both propagating and evanescent waves, contrary to the predictions of the conventional coherence theory, the field coherence length is z dependent. Moreover, we brought the first experimental evidence that the coherence length can have values smaller than the wavelength of radiation[4]. As in the case of the spectral density, the second order near-field correlations depend on the statistical properties of an equivalent planar source of radiation which, in turn, are determined by the physical properties of the random medium. Scanning across the surface with a probe having an appropriate aperture, one can evaluate the field's coherence properties which can then be used to retrieve the characteristics of the medium.

It is worth noting that both measurements of the near-field spectra and of the near-field coherence length could be used to infer properties of the interface. When using the second order correlations, one has to perform spatially-resolved intensity measurements and then evaluate the cross-spectral density function. On the other hand, the near-field spectral measurements do not require scanning; instead, one has to determine the near- and "far-field" spectral densities.

A direct relationship between the measurable statistical properties of the optical field and the surface statistics can be established based on the properties of random fields at a few wavelengths away from the interface, i.e. at distances where the evanescent waves contributions have died out. We have demonstrated that, while the "far-field" spatial coherence length does not depend on the distance from the physical interface, its absolute value relates to the standard deviation of the local slope[5]. This behavior is quite different from the one at much larger distances from the interface where the coherence properties are dominated by the finite size of the scattering media as described by the Van Cittert Zernike's theorem. Conventional coherence theory, on the other hand, assumes infinitely extended sources. Because of the minute dimensions of the probe, the extent of the source in our case is practically infinite and therefore the coherence properties are determined by modifications in the intensity angular distribution. The concept of a homogeneous, planar, infinite source of radiation together with the model for the angular distribution of the radiant intensity describes quantitatively the second-order statistical properties of the field emitted at few wavelengths away from the surface of a random

[5] A. Apostol, A. Dogariu, "Coherence properties near interfaces of random media", Physical Review E, 67, 055601(R) (2003).

medium. Our results elucidated the dependence between the coherence properties in this range and the interface statistics.

We have seen that in the case when light is transmitted through or is emitted within a highly scattering medium, the contrast of the intensity fluctuations is always close to one, independent of the r.m.s height fluctuations of the interface. In this situation, the first-order statistics of intensity, or in other words the speckle contrast, can not be used to infer information about the surface. However, when randomly inhomogeneous media are excited locally, in a illumination-reflection geometry of the near-field microscope for example, we found that the near-field speckle patterns are governed by non-Gaussian statistics and, consequently, their optical contrast is significantly smaller than unity. We have shown experimentally that, the probability density of the scattered intensity depends on the intensity of the incident light and also on the physical properties of the medium. In this situation, the corresponding optical contrast can be used to retrieve information about the surface statistics. We have demonstrated that certain experimental configurations specific to near-field optics may be needed to reveal structural interface details smaller than the wavelength of light, allowing also to account for subsurface effects.

Optical fields in the proximity of random media can be modeled as a superposition of waves with random phases. We have shown that, when the experimental configuration and the type of excitation are properly accounted for, the random walk concept can describe the characteristics of both Gaussian and non-Gaussian regimes encountered in the near-field of random media. In the case of a local excitation of the medium, a simple model of the coherent superposition of waves allows accounting for both surface and subsurface

effects. The experimental dependence of the optical contrast on the surface statistics is also quantitatively explained by the random walk concept and can be used for inferring the properties of the medium[6].

The results included in this thesis prove that the statistical properties of the electromagnetic fields in the close proximity of inhomogeneous surfaces can be used to obtain information about the interface statistics. They also suggest the possibility to adjust the coherence properties of the emitted radiation by modifying the statistical properties of the surface. As illustrated in this thesis, understanding the random interference phenomena in the near-field could also lead to new possibilities for surface and subsurface diagnostics of inhomogeneous media such as, biological cells. In addition, controlling the statistical properties of radiation at subwavelength scales should be of paramount importance in the design of miniaturized optical sources, detectors and sensors.

[6] A. Apostol, A. Dogariu, "Non-Gaussian statistics of optical near-fields", Physical Review E (submitted)

LIST OF REFERENCES

[1] L. Mandel and E. Wolf, Optical Coherence and Quantum Optics, Cambridge University Press, Cambridge, 1995.

[2] Laser Speckle and Related Phenomena, Editor: J.C. Dainty, New York, 1975

[3] B. Shapiro, Phys. Rev. Lett. **57**, 2168 (1986)

[4] I. Freund and D. Eliyahu, Phys. Rev. A 45, 6133 (1992)

[5] W. H. Carter and E. Wolf, J. Opt. Soc. Am. **65**, 1067, (1975).

[6] S. Chandrasekhar, Radiative Transfer, Dover Publications, Inc., New York, 1960.

[7] M. A. Paesler and P. J. Moyer, Near field optics, theory, instrumentation and applications, Wiley-Intersicence ISBN (1996)

[8] B. Hecht, et al., J. Chem. Phys. **112**, 7761 (2000)

[9] D. W. Pojl, W. Denk, and M. Lanz, Appl. Phys. Lett. **44**, 651 (1984)

[10] U. Durig, D. Pohl and F. Rohner, J. Appl. Phys. **59**, 3318 (1986)

[11] E. Betzig, et all, Biophys. J. **49**, 269 (1986)

[12] E. Betzig and J. Trautman, Science , **257,** 189 (1992)

[13] H. Danzebrink, J. Microscopy **176**, 276 (1994)

[14] H. Danzebrink, O. Ohlsson and G. Wilkening, Ultramicroscopy **61**, 131 (1995)

[15] Nano-optics, edited by S. Kawata, M. Ohtsu, M. Irie and M. Ohtsu (Springer Verlag, Berlin, 2002)

[16] D. Courjon, Near-Field Microscopy and Near-Field Optics (London: Imperial college press, 2003)

[17] M. Ohtsu, K. Kobayashi, Optical Near-Fields (Springer Verlag, Berlin, 2004)

[18] Progress in Nano-Electro-Optics, edited by M. Ohtsu I (Springer Verlag, Berlin, 2003)

[19] Paras N. Prasad, Nanophotonics (John Wiley & Sons, Inc 2004)

[20] K. Lieberman, N. Ben-Ami, A. Lewis, Rev. Sci. Instrum., 67, 3567 (1996).

[21] Harootunian A, et al., Appl. Phys. Lett, **49**, 674 (1986).

[22] G. A. Valaskovic, M. Holton and G. H. Morrison, Appl. Optics **34**, 1215 (1995)

[23] H. Heinzelmann, et all, J. Microsc. **194**, 365 (1999)

[24] Toledo-Crow R, et al., Appl. Phys. Lett. **60**, 2957 (1992).

[25] Betzig E, et al., Appl. Phys. Lett. **60**, 2484 (1992).

[26] Lewis A, et al. Spectroscopic Membrane Probes **11**, 81 (1988).

[27] Lewis A, et al., Cell Biology **9**, 70 (1999).

[28] C.M.R. Clancy, et al., J. Phys. Chem. B **104**, 12098 (2000)

[29] H. Muramatsu et al., Materials Science and Engineering C **12**, 29 (2000)

[30] M.F Garcia-Parajo et al., Bioimaging **6**, 43 (1998)

[31] Th. Enderle, et al., Proc. Natl. Acad. Sci. USA **94,** 520 (1997)

[32] Th. Enderle, et al., Ultramicroscopy **71**, 303 (1998)

[33] P. Nagy, et al., Journal of Cell Science **112**, 1733 (1999)

[34] Pandolfi F, et al., Cancer, **69**, 5, 1165 (1992).

[35] Winig BM, et al., Experimental Cell Research, **237**, 2, 364 (1997).

[36] Mariani, et al., FEBS Lett., **406**, 1-2, 83 (1997).

[37] Manenti S, et al., FEBS Lett., **419**, 1, 95 (1997).

[38] Minamiguchi K, et al., International J. of Cancer, **93**, 3, 307 (2001).

[39] Aznavoorian S, et al., J. of Biological Chem., **271**, 6, 3247 (1996).

[40] Hiscox S and Jiang WG., J. of Cell Science, **112**, 18, 308 (1999).

[41] Rosenbaum C, et al., Neurobiology of Disease, **7**, 483 (2000).

[42] Trofatter JA, et al., Cell, **72**, 791 (1993).

[43] Rouleau GA, et al., Nature, **363**, 515 (1993).

[44] Morrison H, et al., Genes & Development, **15**, 968 (2001).

[45] H. Roychowdhury and E. Wolf, Opt. Lett., **28**, 170 (2003).

[46] R. Carminati and J. J. Greffet, Phys. Rev. Lett., **82**, 1660 (1999).

[47] A. V. Shchegrov, K. Joulain, R. Carminati, and J-J Greffet, Phys. Rev. Lett., **85**, 1548 (2000).

[48] T. Setala, M. Kaivola and A. T. Friberg, Phys. Rev. Lett., **88**,123902-1 (2002).

[49] K. P. Gaikovich, A.N. Reznik, V.L. Vaks and N.V. Yurasova, "New effect in near-field thermal emission", Phys. Rev. Lett., **88**,104302-1 (2002).

[50] C. Henkel, K. Joulain, R. Carminati and J.-J. Greffet, Opt. Comm., **186**, 57 (2000).

[51] E.Wolf and W.H.Carter, Opt. Comm., **50**, 131 (1984).

[52] D. G. Fischer, J. Mod. Opt. **47**, 1359 (2000).

[53] W. Goodman, Statistical Optics, J. Wilwy & Sons, Inc., New York, 1985.

[54] A. Dogariu and G. D. Boreman, Opt. Lett., **21**, 701 (1996).

[55] E Wolf and D. F. V. James, Rep. Prog. Phys. **59**, 771 (1996).

[56] H. Roychowdhury and E. Wolf, Opt. Lett., **28**, 170 (2003).

[57] P. Pusey, Photon correlation and Velocimetry (H. Z. Cummins and G. R. Pike, New York, 1977).

[58] E. Jakeman and R. Tough, Adv. Phys. **37**, 471 (1988).

[59] J. Uozumi, T. Asakura, ATTI **25**, 537 (1977).

[60] Richard Barakat, J. Opt. Soc. Am. **71**, 86 (1981).

[61] J. Uozumi, T. Asakura, J. Opt. **12**, 177 (1981).